

ARTICLE

Phagosome resolution regenerates lysosomes and maintains the degradative capacity in phagocytes

Charlene E. Lancaster^{1,2*} , Aaron Fountain^{3,4*} , Roaya M. Dayam^{3,4}, Elliott Somerville³, Javal Sheth¹, Vanessa Jacobelli³, Alex Somerville³, Mauricio R. Terebiznik^{1,2} , and Roberto J. Botelho^{3,4} 

Phagocytes engulf unwanted particles into phagosomes that then fuse with lysosomes to degrade the enclosed particles. Ultimately, phagosomes must be recycled to help recover membrane resources that were consumed during phagocytosis and phagosome maturation, a process referred to as “phagosome resolution.” Little is known about phagosome resolution, which may proceed through exocytosis or membrane fission. Here, we show that bacteria-containing phagolysosomes in macrophages undergo fragmentation through vesicle budding, tubulation, and constriction. Phagosome fragmentation requires cargo degradation, the actin and microtubule cytoskeletons, and clathrin. We provide evidence that lysosome reformation occurs during phagosome resolution since the majority of phagosome-derived vesicles displayed lysosomal properties. Importantly, we show that clathrin-dependent phagosome resolution is important to maintain the degradative capacity of macrophages challenged with two waves of phagocytosis. Overall, our work suggests that phagosome resolution contributes to lysosome recovery and to maintaining the degradative power of macrophages to handle multiple waves of phagocytosis.

Introduction

During phagocytosis, particulates are engulfed and sequestered into phagosomes to aid in infection clearance and tissue homeostasis (Gray and Botelho, 2017; Levin et al., 2016; Henson, 2017; Lancaster et al., 2019). After formation, the innocuous early phagosomes are converted into degradative phagolysosomes by fusing with lysosomes, leading to cargo digestion (Gray and Botelho, 2017; Levin et al., 2016; Fairn and Grinstein, 2012; Pauwels et al., 2017); herein, we will use the term “lysosomes” to include a spectrum of late endosomes, terminal storage lysosomes, and endolysosomes, which are late endosome-terminal storage lysosome hybrids (Bright et al., 2016; Bissig et al., 2017). The phagolysosome thus acquires lysosomal proteins like lysosomal-associated membrane proteins 1 and 2 (LAMP1 and LAMP2), a myriad of hydrolytic enzymes, and the V-ATPase, which acidifies the phagosome (Gray and Botelho, 2017; Levin et al., 2016; Kinchen and Ravichandran, 2010). This ensures digestion of particulates into their primordial components, which are then exported via transporters such as SLC-36.1 (at least in *Caenorhabditis elegans*) or in bulk via vesicular-tubular intermediates (Mantegazza et al., 2014; Gan et al., 2019). The final stage of the life cycle of a phagosome

is now referred to as “phagosome resolution” (Levin et al., 2016; Gray and Botelho, 2017). In unicellular eukaryotes like amoeba, phagosomes containing indigestible material are resolved via egestion, expelling indigestible content and recycling the plasma membrane (Gotthardt et al., 2002; Stewart and Weisman, 1972). While this was assumed to occur in mammalian cells, recent work suggested that phagosomes undergo shrinkage and fission instead (Krajcovic et al., 2013; Krishna et al., 2016; Levin-Konigsberg et al., 2019). Partly, this occurs via processes regulated by the mechanistic target of rapamycin complex 1 (mTORC1) and the lipid kinase PIKfyve (Krajcovic et al., 2013; Krishna et al., 2016). In addition, phosphatidylinositol-4-phosphate [PtdIns(4)P] on phagolysosomes recruits SKIP/PLEKHM2 to secure kinesin motors to lysosomes via the Arl8b GTPase, which collectively drive membrane extrusion via phagosome tubules, aiding in phagosome resolution. Interestingly, ER-phagosome contact sites formed via Rab7 and the oxysterol-binding protein-related protein 1L transfer phagosomal PtdIns(4)P to the ER for turnover of PtdIns(4)P from resolving phagolysosomes (Levin-Konigsberg et al., 2019).

Surprisingly, little else is known about phagosome resolution, including how the phagosomal membrane is recycled or

¹Department of Biological Sciences, University of Toronto at Scarborough, Toronto, Ontario, Canada; ²Department of Cell and Systems Biology, University of Toronto, Toronto, Ontario, Canada; ³Department of Chemistry and Biology, Ryerson University, Toronto, Ontario, Canada; ⁴Graduate Program in Molecular Science, Ryerson University, Toronto, Ontario, Canada.

*C.E. Lancaster and A. Fountain contributed equally to this work; Correspondence to Roberto J. Botelho: rbotelho@ryerson.ca; Mauricio R. Terebiznik: mauricio.terebiznik@utoronto.ca.

© 2021 Lancaster et al. This article is distributed under the terms of an Attribution–Noncommercial–Share Alike–No Mirror Sites license for the first six months after the publication date (see <http://www.rupress.org/terms/>). After six months it is available under a Creative Commons License (Attribution–Noncommercial–Share Alike 4.0 International license, as described at <https://creativecommons.org/licenses/by-nc-sa/4.0/>).

how phagocytes retune their endomembrane state after degradation of phagosomal contents. For long-lived macrophages (van Furth and Cohn, 1968; Parihar et al., 2010), “free” lysosomes and other membranes must be replenished to allow these cells to degrade multiple rounds of internalized cargo over their lifetimes, though it is unknown if and how lysosomes are reformed after phagosome maturation.

In this study, we report that phagosomes in macrophages undergo fission, tubulation, and splitting, culminating in phagosome fragmentation to reform lysosome-like organelles. We show that phagosome fragmentation required particle digestion, the actin and microtubule cytoskeleton systems, and clathrin. Moreover, we show that a first wave of phagocytosis reduced the number of free lysosomes and abated the degradative activity in phagosomes formed during a second round of phagocytosis. Importantly, given enough time, free lysosomes were replenished, and degradative activity within subsequent phagosomes was recovered in a clathrin- and biosynthetic-dependent manner. Overall, our study reveals a role of phagolysosome resolution in the reformation of lysosomes for reuse by macrophages to sustain multiple rounds of phagocytosis.

Results

Phagolysosomes with undigestible particulates are not egested

Despite numerous studies on phagosomal dynamics, the terminal fate of the phagolysosome remains obscure. For years, phagocytosis was assumed to end with the exocytosis of the phagolysosome and egestion of debris, a notion that likely arose from studies on phagotrophic protozoans (Clarke et al., 2002; Maniak, 2003; Stewart and Weisman, 1972; Gotthardt et al., 2002). Yet, recent evidence suggests that mammalian phagosomes containing degradable cargo, like apoptotic cells or RBCs, undergo shrinkage and/or fission (Krajcovic et al., 2013; Levin-Konigsberg et al., 2019). To investigate if phagolysosomes containing indigestible material are secreted in mammals, we allowed RAW 264.7 macrophages to internalize IgG-opsonized latex beads and followed the nondegradable cargo over 24 h by live-cell imaging. Over this period, we did not observe release of phagosome-sequestered beads (Fig. 1, A and B; and Video 1). Additionally, ionomycin, a calcium ionophore that induces exocytosis (Jans et al., 2004; Xu et al., 2012), did not cause the egestion of beads from macrophages (Fig. S1, A and B), despite activating PLC (Botelho et al., 2000b; Fig. S1 C). Altogether, phagosomes containing nondegradable beads are retained inside mammalian macrophages instead of undergoing exocytosis.

Phagolysosomes containing bacterial cargo undergo fragmentation

Recently, efferosomes and RBC-containing phagosomes were observed to undergo shrinkage and fragmentation (Krajcovic et al., 2013; Levin-Konigsberg et al., 2019). As these particulates are noninflammatory, we thus queried whether phagosomes containing bacteria, which provoke an inflammatory response, would suffer a similar fate. We first used PFA-killed filamentous *Legionella pneumophila* (herein *Legionella* or *Lp*)

expressing mCherry to track large phagosomes by live-cell imaging (Prashar et al., 2013). We used mCherry fluorescence as a proxy for the fate of phagosomes. Interestingly, within 7–20 h, the bacterial filaments collapsed into spheroidal bodies, and there was a gradual increase in cytoplasmic puncta labeled with mCherry (Fig. 1 C and Video 2).

We further investigated this phenomenon by following PFA-fixed mRFP1-*Escherichia coli*-containing phagosomes (Fig. 1 D and Video 3) because *E. coli* are quasi-homogeneous in shape and mRFP1 is resistant to degradation (Katayama et al., 2008). Using fluorescence and volume thresholding to differentiate between phagosomes and phagosome-derived puncta, we calculated the total volume of phagosomes and the total volume of phagosome-derived vesicles (PDVs) per cell over time (see Materials and methods). The total volume of phagosomes per macrophage decayed quadratically, while the total volume of PDVs increased exponentially over time, suggesting correspondence in the two phenomena (Fig. 1, E and F). Using fixed-cell, population-based assays, we similarly found that the number of intact *E. coli* remaining within macrophages decreased over time, while the number of puncta increased (Fig. 1, G–I).

To assess if phagosomes fragmented even when they carried indigestible material, we prepared a semi-degradable cargo by aggregating fluorescently labeled 100-nm polystyrene nano-beads using IgG. We presumed that these bead clumps would be broken apart through IgG proteolysis within the phagolysosome. Indeed, internalized bead clumps gradually formed a cloud of fluorescence or smaller puncta, suggesting that these phagosomes split into smaller components (Fig. S1 D and Video 4). Thereby, these experiments reveal that phagolysosomes containing indigestible yet modular particulate cargo can undergo fragmentation.

Finally, while wholesale phagosomes did not appear to exocytose, we assessed if phagosome-derived content could be secreted. We fed mRFP1-*E. coli* to macrophages for 1 h and chased for an additional 1, 6, or 24 h before collecting media and cell lysates. Probing cell lysates by Western blotting, we observed mostly intact mRFP1 at 1 h after phagocytosis and the accumulation of a cleaved mRFP1 product at 6 and 24 h after phagocytosis, likely generated by phagosome proteases (Fig. S1, E and F). We then evaluated the presence of mRFP1 and GAPDH in cell media, the latter used to control for macrophage death. At 1 h after phagocytosis, there was little mRFP1 in the medium, but at 6 and 24 h, cleaved mRFP1 was observable. By normalizing to GAPDH, cleaved mRFP1 appears to preferentially accumulate in media at 6 h versus 1 h relative to GAPDH, suggesting that phagosomal cargo can be secreted (Fig. S1, E and F).

Phagolysosome fragmentation is dependent on cargo degradation and the cytoskeleton

We next sought to understand some of the prerequisites for phagosome resolution. First, we hypothesized that phagosome resolution requires cargo degradation. To test this, we used either a protease inhibitor cocktail or an NH_4Cl /concanamycin A (Con A) mixture to alkalize the lysosomal pH (Naufer et al., 2018; Li et al., 2013). Vehicle-treated cells increased their PDV volume 4 h after phagocytosis relative to 1 h after phagocytosis,

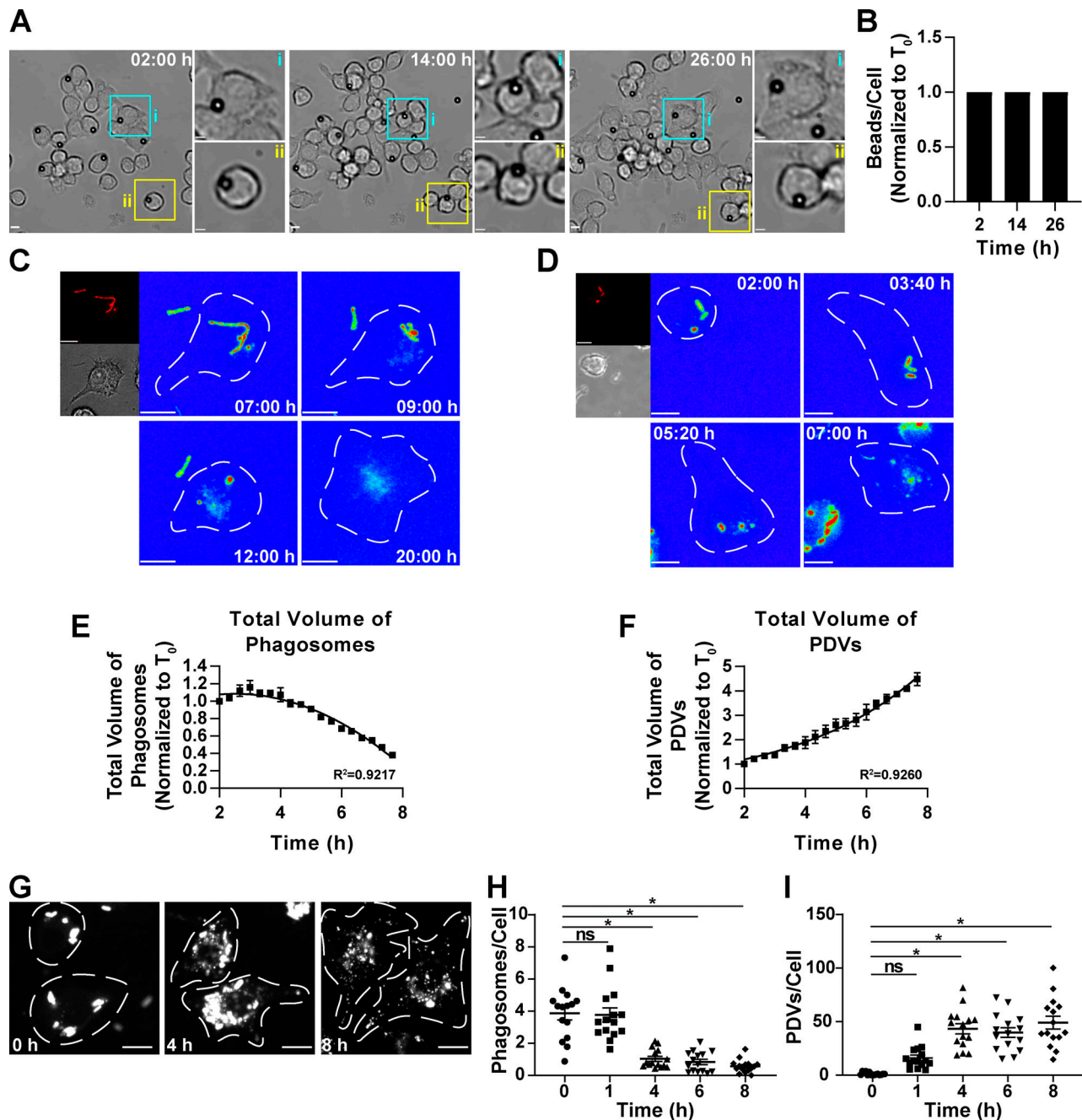


Figure 1. Phagolysosomes undergo fragmentation instead of exocytosis. (A) IgG-opsonized beads in RAW cells tracked for 24 h. Shown are differential interference contrast (DIC) images. Boxes indicate areas enlarged in (i) and (ii). **(B)** Number of beads in macrophages over time and normalized to T_0 . Data are shown as mean \pm SEM from three independent experiments with eight cells quantified per experiment. **(C, D, and G)** Macrophages engulfed filamentous mCherry-Lp for 7 h (C) or mRFP1-E. coli for 2 h (D and G) and then imaged. Dashed lines show cell contours. Main panels in C and D show the red channel in a rainbow scale; red and blue are the highest and lowest intensity levels, respectively. Smaller panels show the red and DIC channels for the first frame. **(E and F)** Total volume of phagosomes and PDVs per cell over time are shown as mean \pm SEM of 3 independent experiments with 10–25 cells analyzed per experiment. Volumes were normalized to T_0 . **(H and I)** Quantification of the number of PDVs and intact phagosomes. Data are mean \pm SEM of 3 independent experiments with 15 images quantified per time point. One-way ANOVA with Tukey’s test was used to compare each time point against T_0 (*, $P < 0.05$). See corresponding [Video 1](#), [Video 2](#), and [Video 3](#). Scale bars: 10 μ m (main panels), 5 μ m (insets).

consistent with phagosome fragmentation (Fig. 2, A–D). In comparison, cells treated with the protease cocktail or the NH_4Cl /Con A mixture had lower PDVs 4 h after phagocytosis relative to the corresponding control cells (Fig. 2, A–D). Thus, cargo degradation is necessary for phagolysosome fragmentation.

We then assessed the role of the cytoskeleton in phagosome fragmentation since the cytoskeleton is implicated in membrane scission (Damiani and Colombo, 2003; Gautreau et al., 2014; Ripoll et al., 2018; Bezanilla et al., 2015). To assess this, macrophages internalized mRFP1-E. coli for 40 min and were then

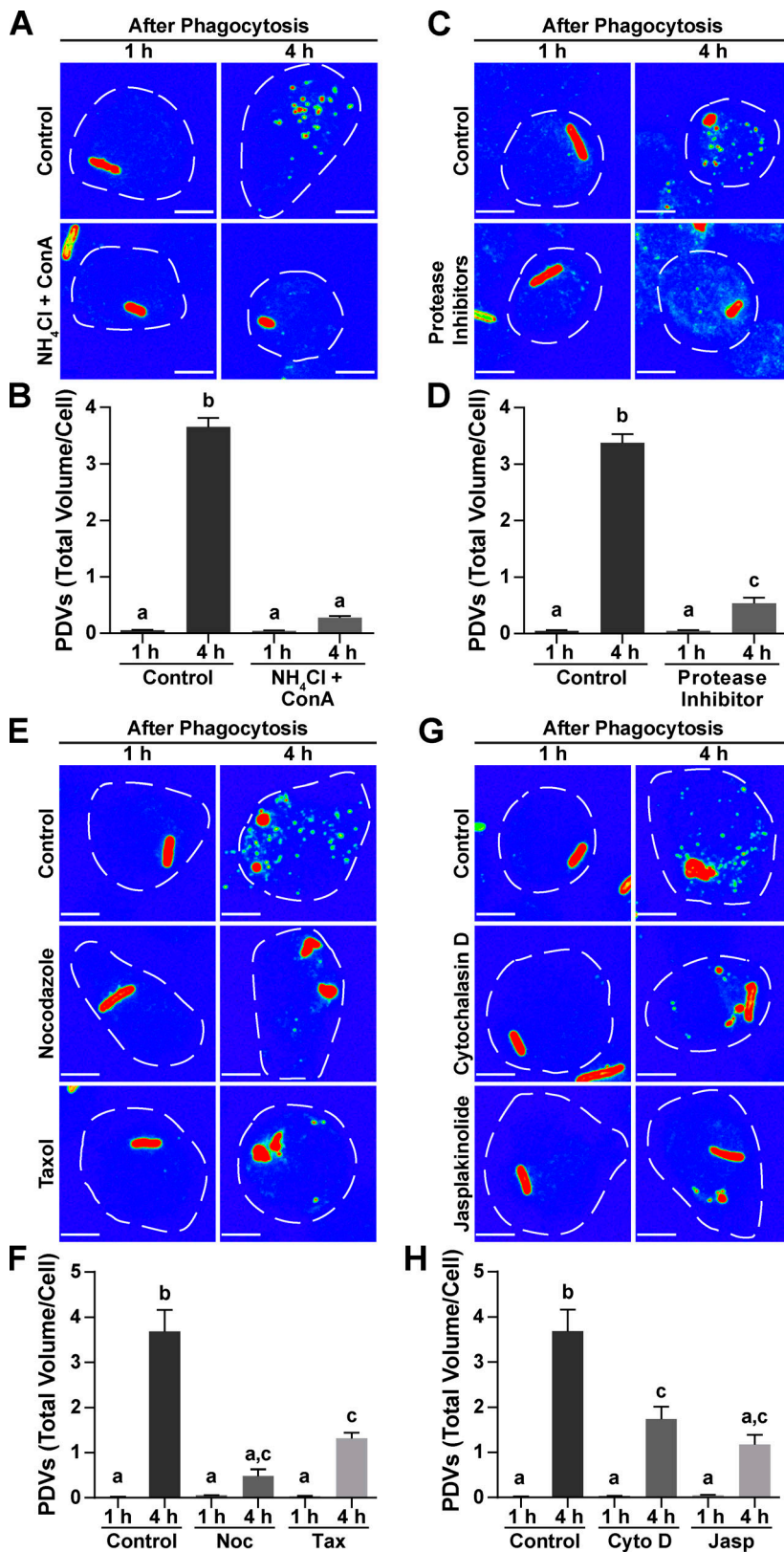


Figure 2. Fragmentation of the phagolysosome requires cargo degradation and the cytoskeleton. (A, C, E, and G) Macrophages engulfed *E. coli* for 15 min, chased for 25 min, and treated with either Con A and NH₄Cl (A), protease inhibitor cocktail (C), microtubule inhibitors (E), actin inhibitors (G), or vehicle control (DMSO). Cells were fixed after 1 or 4 h after phagocytosis and stained with an anti-*E. coli* antibody whose fluorescence is displayed in rainbow scale. Dashed lines show cell contours. Scale bars: 5 μm. (B, D, F, and H) Total volume of PDVs per cell. Data are mean ± SEM of 3 independent experiments with 25 cells quantified per condition of an experiment and compared by one-way ANOVA with Tukey's test. Conditions labeled with different letters (a–d) are statistically different (P < 0.05).

treated with the actin- and microtubule-stabilizing drugs jasplakinolide and Taxol, respectively, or with cytochalasin D or nocodazole to depolymerize actin or microtubules, respectively. Unlike control conditions, all these drugs

significantly lowered PDV volume at 4 h after phagocytosis (Fig. 2, E–H). Therefore, the actin and microtubule cytoskeletons are required for efficient fragmentation of the phagolysosome.

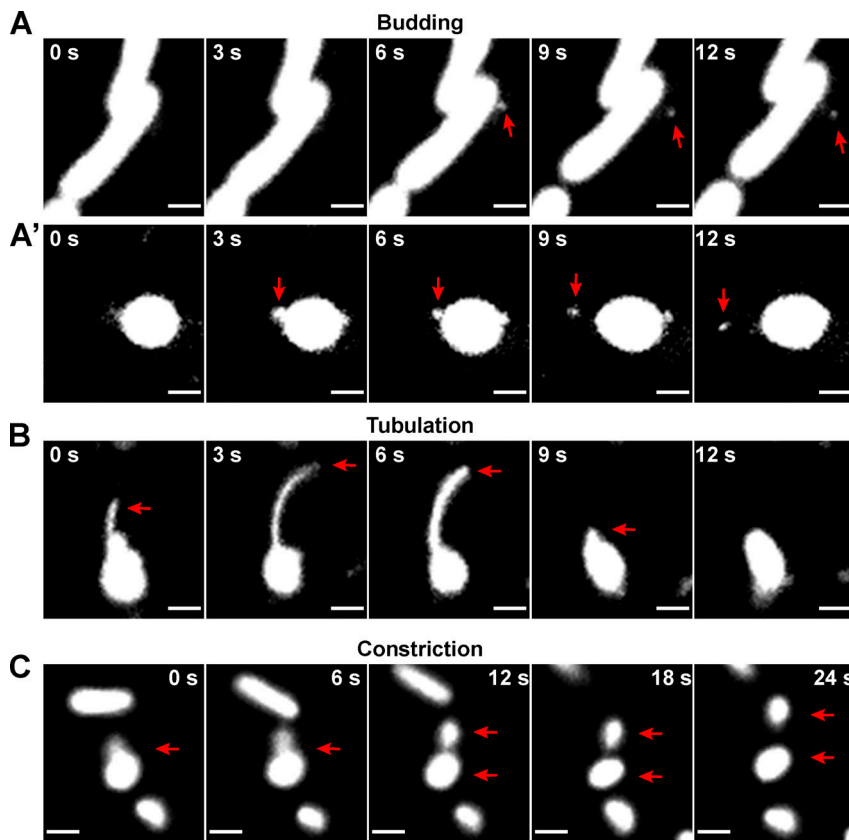


Figure 3. Phagosomes undergo different modes of fragmentation. Macrophages engulfed mRFP1-*E. coli* for 1 h, were chased for 3 h to elicit fragmentation, and then were imaged live for 10-min intervals at a frequency of one frame every 3 s. **(A and A')** Vesicle budding in phagosomes with intact *E. coli* rods (A, early budding) or after fragmentation (A', late budding). **(B and C)** Tubulation events producing small phagosomal fragments or retracting into the phagosome (B) and constrictions forming large phagosomal fragments (C). Red arrows track single events described above. See corresponding Videos 5, 6, 7, and 8. Scale bars: 2 μ m.

Clathrin is necessary for resolution of the phagolysosome

We next studied the dynamics of phagosomal fragmentation and observed fission events that generated vesicles (Fig. 3, A and A'; and Videos 5 and 6), tubules that either scissioned or collapsed back into the original organelle (Fig. 3 B and Video 7), or constriction events that generated large fragments rather than small vesicles (Fig. 3 C and Video 8). This suggests multiple mechanisms of phagosomal fragmentation.

Clathrin is an important mediator of vesicle budding, known for its role in endocytosis and export from the trans-Golgi network (Kirchhausen et al., 2014). However, clathrin is also involved in budding at the endosome, lysosome, and autolysosomes (Stoorvogel et al., 1996; Traub et al., 1996; Rong et al., 2012). We thus investigated if clathrin is required for phagosomal fragmentation. We observed clathrin during phagosomal maturation and resolution by live-cell imaging of RAW macrophages expressing a GFP fusion of the clathrin light chain (CLC-GFP). This revealed clusters of clathrin localized in close proximity to phagolysosomes containing *Lp* (Fig. 4 A) or beads (Fig. S2 A). Quantifying the frequency of clathrin puncta associated with fission events was challenging, given the heterogeneity of phagosomal resolution caused by varying phagosomal age, the three-dimensionality of phagosomes, the ephemeral nature of clathrin puncta, and photobleaching. Yet, we observed that clathrin puncta cooccurred in 38 fission events out of 55, or ~70% of the fission events (Fig. 4, B and C; and Video 9). In addition, we found clathrin patches on PFA-fixed, isolated phagosomes immunostained for LAMP1 and clathrin, evincing that clathrin is physically associated with phagosomes (Fig. 4 D).

We then evaluated the role of clathrin in phagosomal fragmentation. To avoid interference with phagocytosis or phagosomal maturation that might compromise phagosomal resolution, we inhibited clathrin in macrophages with two inhibitors, Pitstop 2 and ikarugamycin, after 40–60 min of phagosomal maturation (von Kleist et al., 2011; Elkin et al., 2016). Using live-cell imaging of *Lp*-containing phagosomes, we found that phagolysosomes in Pitstop-treated cells did not collapse to the same extent as in control cells, nor was there an increase in the volume of PDVs over many hours after phagocytosis (Fig. 5, A and B; and Video 10). Similarly, we observed a significant reduction in PDVs in Pitstop- and ikarugamycin-treated cells 4–8 h after phagocytosis of *E. coli*, quantified by puncta volume (Fig. 5, C and D) and particle number (Fig. S2, B–E). Additionally, we used a rapamycin-induced dimerization system that acutely displaces clathrin to mitochondria (Robinson et al., 2010; Robinson and Hirst, 2013). Satisfyingly, this treatment impaired phagosomal fragmentation relative to control conditions (Fig. 5, E and F). To determine that these observations were not constrained to RAW cells, we showed phagosomal fragmentation in primary macrophages that engulfed mRFP1-*E. coli* and that this was impaired by Pitstop or ikarugamycin (Fig. S2, F and G).

The large GTPase dynamin is essential for clathrin budding because it catalyzes the scission of clathrin-coated vesicles from cellular membranes (Mettlen et al., 2009). To assess dynamin involvement in the resolution of phagosomes, we used two dynamin inhibitors, dyngo-4a and dynole 34-2 (Hill et al., 2009; McCluskey et al., 2013). Dynole 34-2- or dyngo-4a-treated cells

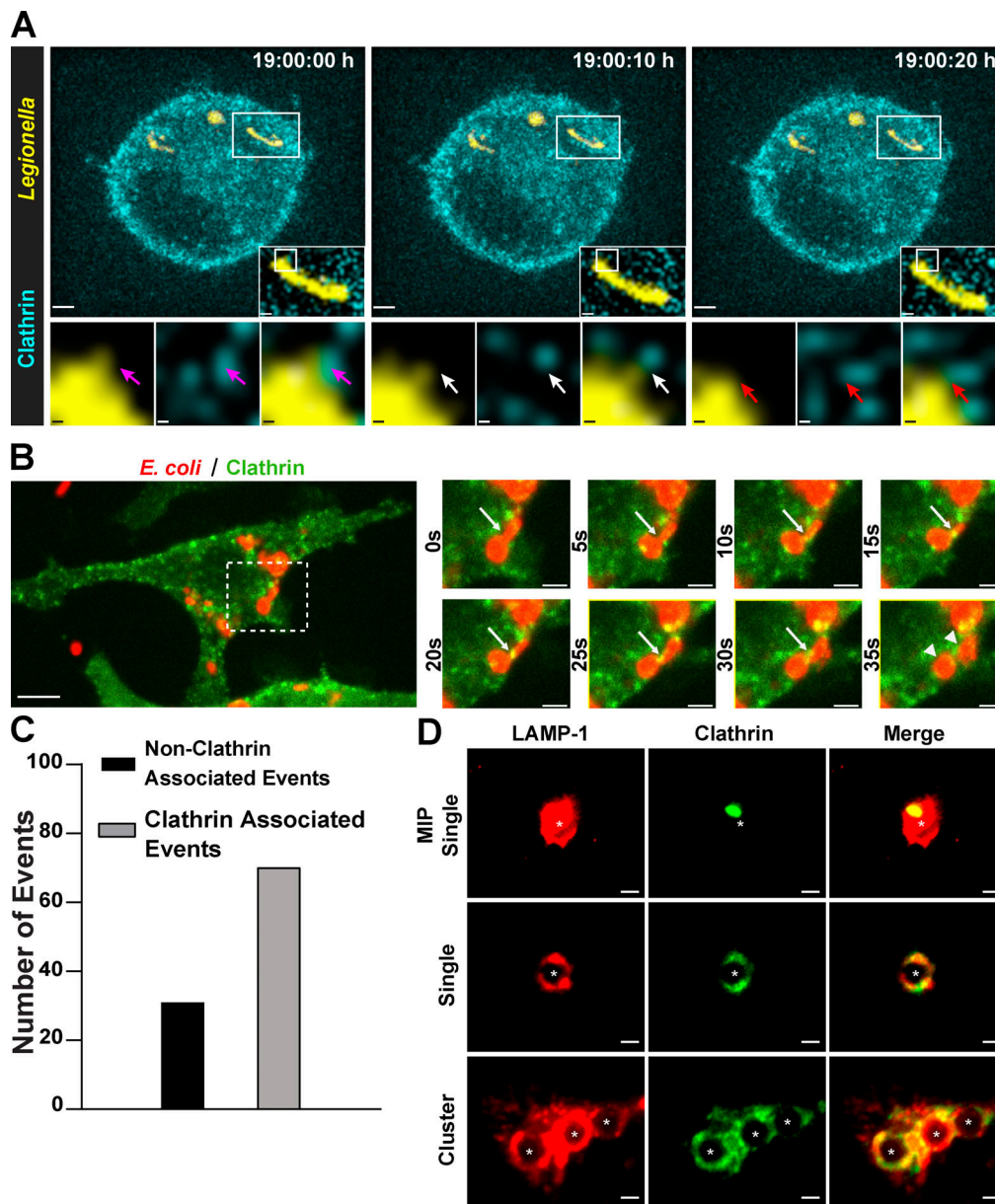


Figure 4. Clathrin localizes to the phagolysosome. (A and B) Macrophages expressing clathrin-GFP were imaged live after uptake of mCherry-*Lp* (A) or mRFP1-*E. coli* (B) for >1 h. For A, deconvolved, collapsed z-stacks are shown, while insets/lower panels are deconvolved single z-planes. Boxes indicate areas enlarged in the insets/lower panels. Arrows show clathrin in close association with *Lp*. Scale bars: 2 μm (main panels), 0.5 μm (insets), 0.1 μm (lower panels). For B, arrows show fission associated with clathrin puncta, and arrowheads show fragments after fission. See corresponding Video 9. Scale bars: 5 μm (main panel), 2 μm (insets). **(C)** Quantification of fission events associated with clathrin. **(D)** Isolated and fixed phagosomes (asterisks) were immunolabeled for LAMP1 (red) and clathrin (green). Top row: A z-stack of a single phagosome projected as the MIP. Middle row: Single-plane image of isolated phagosome showing clathrin patches. Bottom row: Cluster of phagosomes coisolated. Images are representative of 24 phagosomes analyzed. Scale bars: 2 μm .

produced a significantly smaller total volume of PDVs than control cells 4 h after phagocytosis (Fig. S3). Collectively, clathrin machinery mediates the resolution of the phagolysosome.

PDVs have lysosomal characteristics

To investigate if PDVs retained a predominant lysosomal character, we looked at their association with endolysosomal markers. Macrophages were challenged with ZsGreen-*E. coli* for 6 h to elicit phagosome fragmentation, then fixed and

immunostained against LAMP1 and LAMP2. Approximately 80% of PDVs (defined as ZsGreen-positive compartments with an area >0.1 μm^2 but <4 μm^2 to exclude the parental phagosomes) were positive for LAMP1 and LAMP2 (Fig. 6, A and B). Subsequently, we determined that >80% of PDVs were acidic and proteolytically active by using LysoTracker Red and Magic Red Cathepsin L fluorogenic substrate, respectively (Fig. 6, C-F). Altogether, phagolysosome-derived compartments predominantly retain endolysosomal features of the mother phagolysosome.

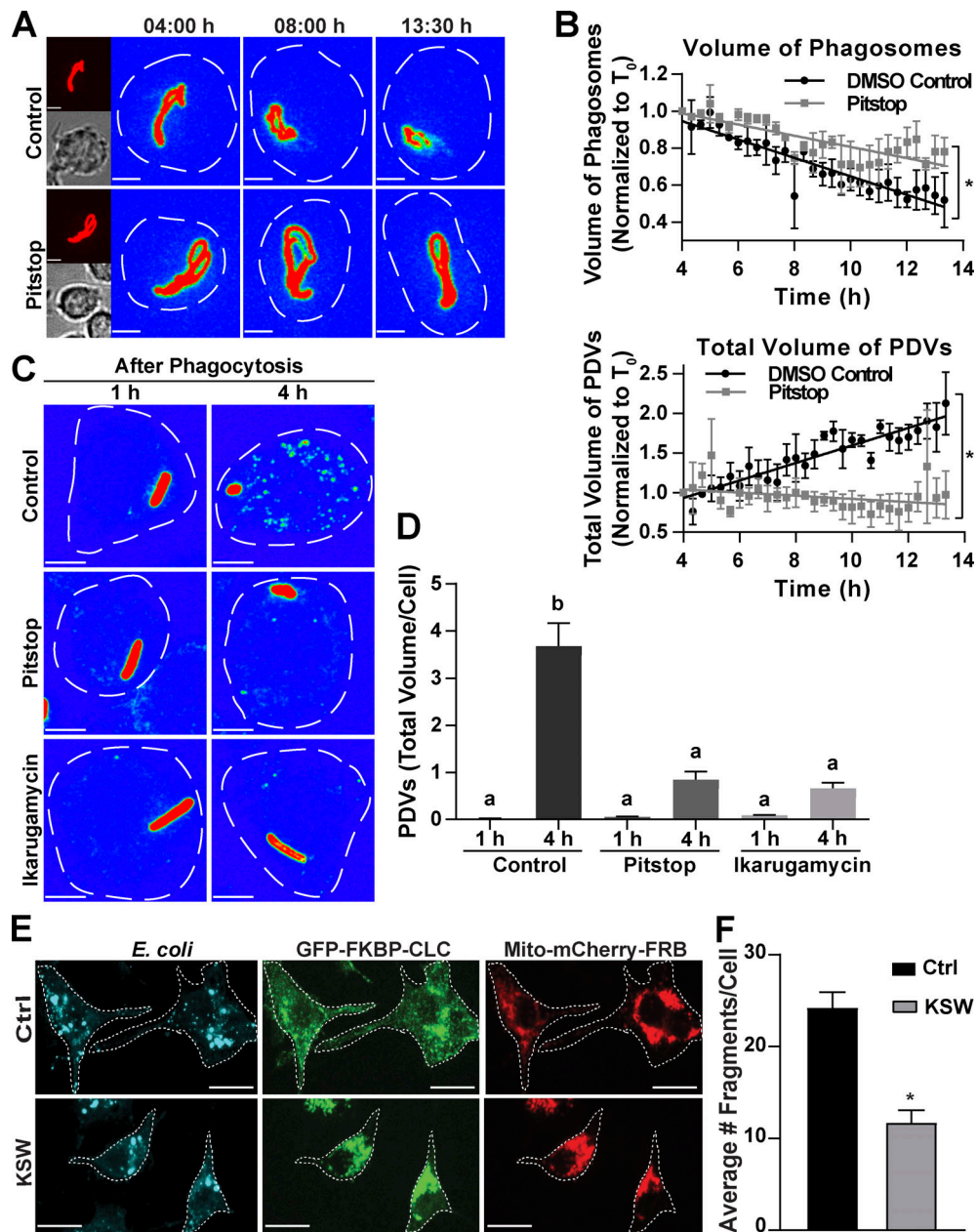


Figure 5. **Clathrin is necessary for the resolution of the phagolysosome.** (A) Imaging of RAW cells 4 h after phagocytosis of mCherry-*Lp* (rainbow scale). Pitstop was added 10 min before imaging. See corresponding [Video 10](#). Scale bars: 5 μ m. (B) Quantification of the volume of phagosomes and PDVs over time. Volumes were normalized to T_0 for each treatment. Data are mean \pm SEM of three independent experiments. *, $P < 0.05$ indicates that the regressions are significantly different. (C) RAW cells engulfed mRFP1-*E. coli* for 15 min, chased for 25 min, and treated with Pitstop or ikarugamycin. Cells were fixed 1 or 4 h after phagocytosis and immunostained against *E. coli* (rainbow scale). Scale bars: 5 μ m. (D) Volume of PDVs per cell for experiments shown in C. Data are mean \pm SEM of 3 independent experiments with 25 cells quantified per condition of an experiment, and results were tested by one-way ANOVA with Tukey's test. Different letters indicate results are statistically different ($P < 0.05$). (E) RAW cells expressing Mito-mCherry-FRB and GFP-FKBP-CLC were treated with rapamycin to induce knocksideways (KSW) of the clathrin light chain or DMSO (Ctrl) and allowed to internalize *E. coli*. Cells were fixed 3 h after phagocytosis, stained for *E. coli*, and imaged. Scale bars: 10 μ m. (F) Number of fragments stained with anti-*E. coli* antibodies in control and rapamycin-treated cells. Data are mean \pm SEM of three independent experiments and statistically tested using an unpaired *t* test (*, $P < 0.05$). Dashed lines show cell contours (A, C, and E).

Phagolysosome fragmentation reforms lysosomes

Phagosomes fuse and thus consume free lysosomes, which may exhaust the degradative capacity of the phagocyte. Given the macrophage long lifespan and capacity to undertake successive rounds of phagocytosis (Cannon and Swanson, 1992; Parihar et al., 2010; van Furth and Cohn, 1968), we postulated that

phagosome fragmentation may participate in lysosome reformation and maintaining the degradative capacity of macrophages.

To test this hypothesis, we assessed the number of LAMP1-positive puncta as a proxy for free lysosomes in resting macrophages or after phagocytosis of indigestible latex beads, precluding

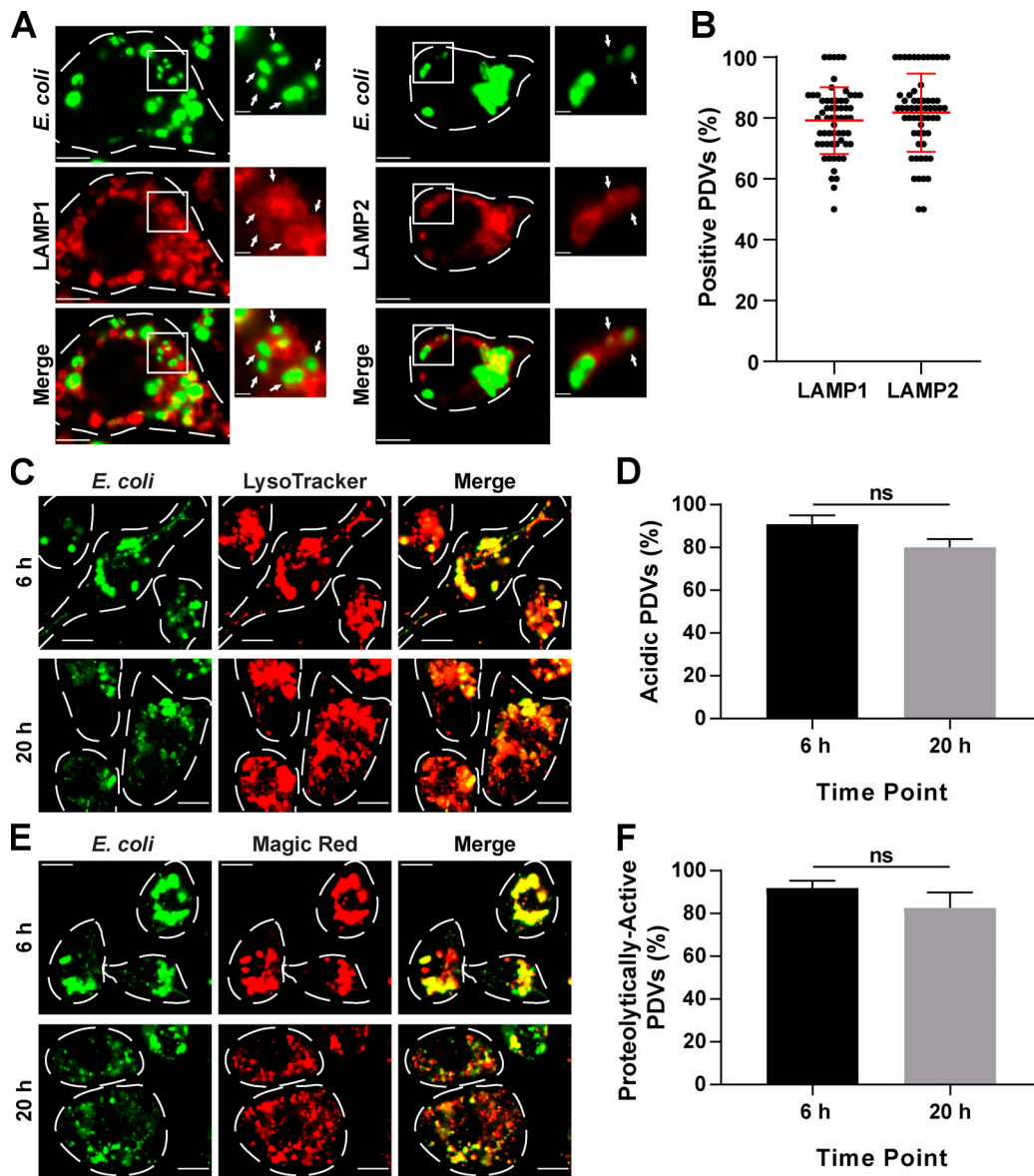


Figure 6. PDVs exhibit lysosomal properties. (A) Macrophages were challenged with ZsGreen-*E. coli* for 6 h, fixed, and stained for LAMP1 or LAMP2. Arrows indicate colocalization of LAMP1 or LAMP2 to PDVs. Scale bars: 5 μ m (main panels), 1 μ m (insets). (B) Percentage of PDVs positive for LAMP1/LAMP2. Data are mean \pm SD of 60 cells from 3 independent experiments. (C and E) PDVs from ZsGreen-*E. coli* phagosomes visualized at 6 and 20 h after phagocytosis in cells stained with LysoTracker Red (C) or Magic red (E) for 1 h before live-cell imaging. Scale bars: 10 μ m. Dashed lines show cell contours (A, C, and E). (D and F) PDVs were scored for co-occurrence with LysoTracker Red (D) or Magic Red (F) using images as shown in C and E, respectively. Data are mean \pm SEM of 3 independent experiments with 25–70 cells quantified per time point of an experiment. Data were statistically analyzed by an unpaired t test.

phagosome resolution. We saw significantly fewer free lysosomes in macrophages that engulfed latex beads and undertook phagosome maturation (60 min) relative to resting macrophages or macrophages with immature phagosomes (15 min; Fig. 7, A and B). In comparison, there was no apparent difference in free lysosome number between resting macrophages and those with immature phagosomes (15 min), consistent with low phagosome-lysosome fusion and demonstrating that our quantification method was not affected by bead crowding in the cytoplasm (Fig. 7, A and B).

To determine if phagosome resolution aids in lysosome regeneration, we then employed *Lp*; these form extensive phagosomes that do not overcrowd the cytoplasm because of coiling,

facilitating visualization of lysosome number. Free lysosomes were quantified by applying a mask on fluorescent *Lp* and quantifying the number of LAMP1-positive puncta outside of this mask. We compared resting cells and cells with *Lp*-containing phagosomes for 2 h or 6 h after phagocytosis to elicit phagosome-lysosome fusion (2 h) and fragmentation (6 h), respectively. As with bead-containing phagosomes, cells that were incubated for 2 h after phagocytosis suffered a 45% reduction in the number of free lysosomes (Fig. 7, C and D). Interestingly, and relative to 2 h after phagocytosis, we observed a bounce in the number of free lysosomes after the onset of phagosomal fission (6 h; Fig. 7, C and D), suggesting that

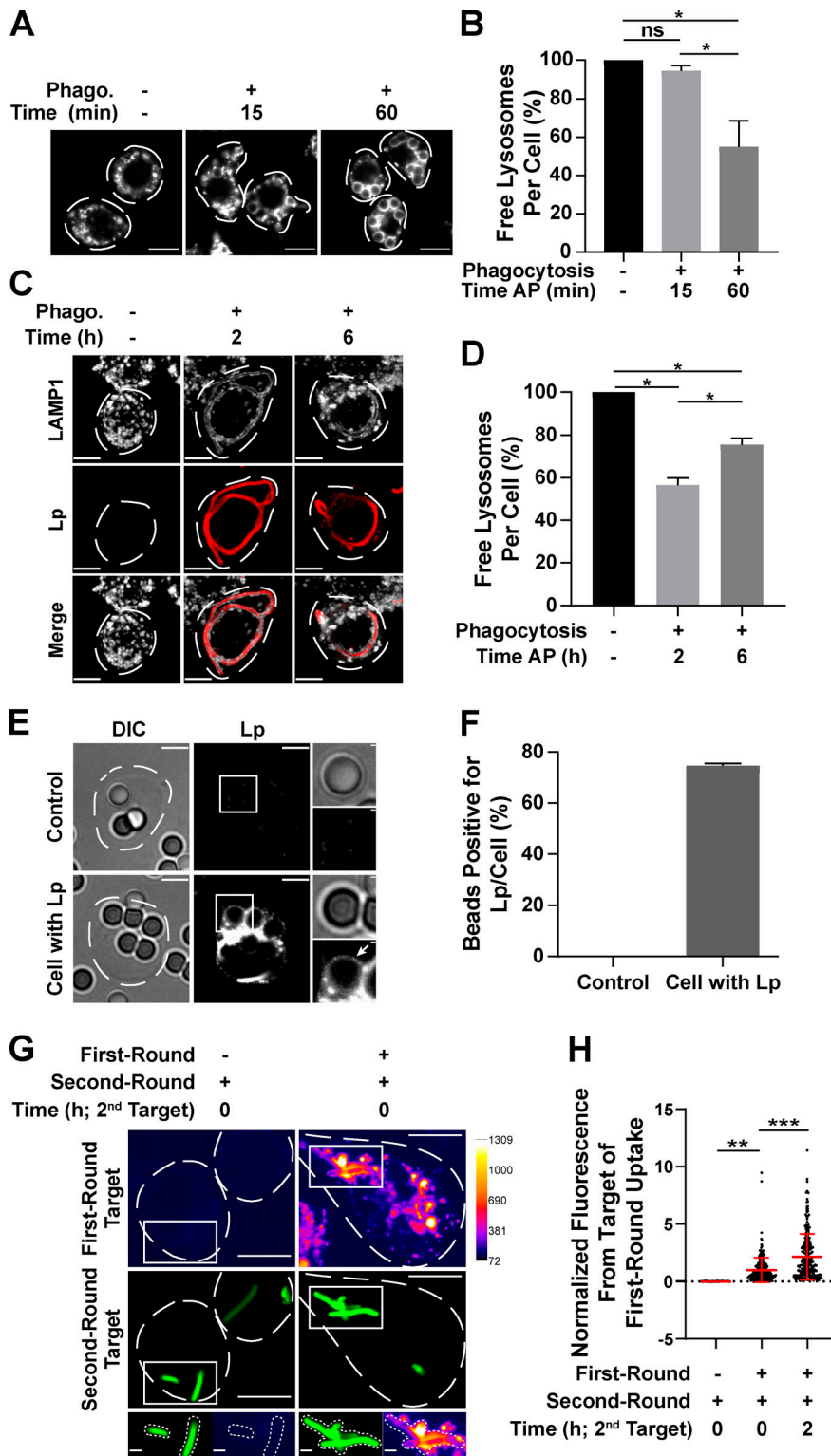


Figure 7. Phagosome (Phago.) maturation consumes free lysosomes. (A and C) Macrophages were challenged with IgG beads (A) or mCherry-*Lp* (C) and stained for LAMP1 and *Lp*. Images show LAMP1 (A and C) and *Lp* (C). Scale bars: 10 μ m (A), 5 μ m (C). **(B)** Number of free lysosomes per cell at specified times after phagocytosis (Time AP) for images described in A. **(D)** Number of free lysosomes per cell at specified times after phagocytosis (Time AP) for images described in C. In B and D, data are mean \pm SEM of 3 independent experiments, where 60 cells (B) and 20 cells (D) were quantified per condition in each experiment, normalized to resting cells, and tested by one-way ANOVA with Tukey's test (*, $P < 0.05$). **(E)** RAW cells that engulfed *Lp* were chased 6 h to allow for *Lp* fission and presented for 1 h with IgG-opsonized beads (second round of phagocytosis). Cells were fixed and stained for *Lp*. The arrow shows bacterial debris in the bead phagosome. Scale bars: 5 μ m (main panels), 0.5 μ m (insets). **(F)** Percentage of beads that were positive for *Lp* fragments in E. Data are mean \pm SEM of 3 independent experiments with 20 cells quantified for each condition per experiment. **(G)** Macrophages were presented with mRFP1-*E. coli* for 7 h as a first round of phagocytosis before being challenged with ZsGreen-*E. coli* for a second round of uptake. As a control, resting cells were challenged only with one round of phagocytosis using ZsGreen-*E. coli*. Scale bars: 10 μ m (main panels), 2 μ m (insets). **(H)** Quantification of mean mRFP1 fluorescence intensity (derived from first-round phagosomes) on ZsGreen-*E. coli*-containing phagosomes (second-round phagosomes) as described in G. Data were normalized to macrophages without the first wave of phagocytosis and presented as mean \pm SD of 148–348 cells across 3 independent experiments. Conditions were compared statistically using one-way ANOVA with Tukey's test (**, $P < 0.01$; ***, $P < 0.001$). Dashed lines show cell contours (A, C, E, and G).

macrophages began to recover lysosomes through phagosomal fragmentation.

We next hypothesized that phagosome-derived, lysosome-like compartments can fuse with subsequent phagosomes. To test this, we challenged macrophages with two rounds of phagocytosis. In one model, we allowed macrophages to engulf PFA-killed, mCherry-expressing *Lp* followed by a 6-h chase to

prompt phagosome resolution. We then challenged these macrophages to engulf latex beads followed by 1 h of maturation. We observed transfer of *Lp*-derived debris (first phagocytosis) into bead-containing phagosomes (second phagocytosis; Fig. 7, E and F). In a second model, macrophages were first allowed to form phagosomes containing mRFP1-*E. coli* (first phagocytosis) for 1 h, and either immediately (0 h) or after 2 h to begin phagosome

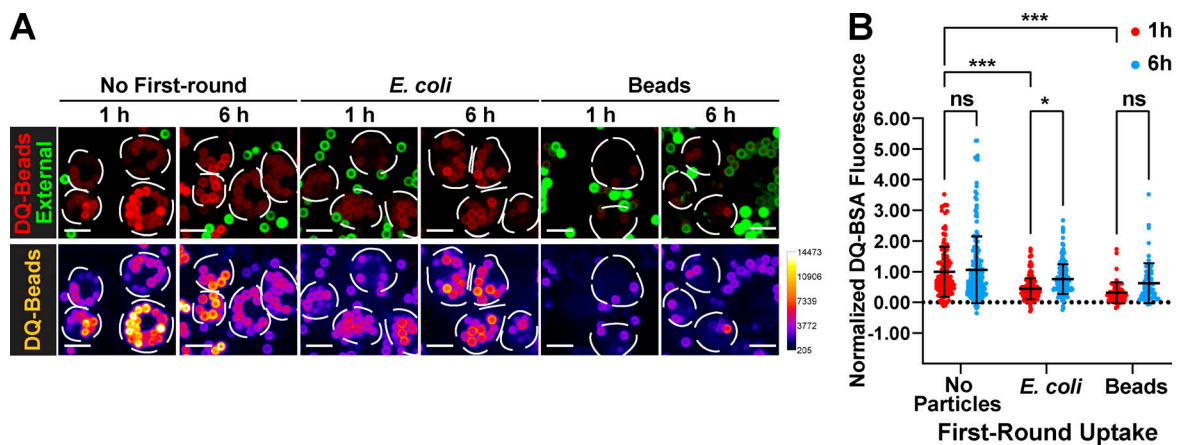


Figure 8. Phagosome resolution recovers degradative capacity in macrophages. (A) Macrophages were given no particles or allowed to engulf for 1 h unlabeled *E. coli* or unlabeled IgG-opsionized beads for the first round of phagocytosis, followed by 1 h or 6 h to elicit maturation/resolution, before the addition of DQ-BSA-opsionized beads for a second round of engulfment. External beads were immunostained (green), and cells were imaged live. Lower panels show the red channel (DQ-BSA) in fire scale. Scale bars: 10 μ m. (B) Quantification of DQ-BSA fluorescence intensity of internalized DQ-BSA beads from experiments described in A. The intensity of each internal DQ-BSA bead was corrected by subtracting the mean intensity of external DQ-BSA beads. Data are presented as mean \pm SD normalized to the mean of 1 h per vehicle condition and are based on 6 independent experiments with 150–503 cells quantified per condition: *, $P < 0.05$; ***, $P < 0.001$.

resolution, the cells were then challenged with ZsGreen-expressing *E. coli* (second phagocytosis) and chased for 1 h to elicit maturation. Using this model, macrophages that were given time to resolve the first phagosomes exhibited a higher degree of mRFP1 colocalization with subsequent phagosomes than macrophages deprived of a chase time period (Fig. 7, G and H). Altogether, these observations suggest that PDVs fuse with subsequent phagosomes, consistent with these being lysosome-like.

Clathrin-mediated phagosome fragmentation is required to recover degradative capacity

Since phagosomes consume lysosomes, we surmised that this may reduce the degradative capacity of phagosomes produced in subsequent rounds of phagocytosis. In turn, subsequent phagosomes may exhibit lower degradative activity than their predecessors. To test this hypothesis, we challenged macrophages with two rounds of phagocytosis. In the first round, macrophages engulfed either IgG-opsionized latex beads or *E. coli*, followed by a second phagocytic wave using IgG-opsionized beads coated with the fluorogenic protease substrate dye-quenched BSA (DQ-BSA). We observed that the fluorescence of DQ-BSA-coated beads was lower in those macrophages that internalized one prior round of beads or *E. coli* 1 h earlier compared with macrophages with no prior phagocytosis (Fig. 8, A and B, red dots in mock primary versus red dots in 1-h *E. coli* or 1-h beads). Importantly, the proteolytic activity of DQ-BSA phagosomes formed during the second round of phagocytosis recovered significantly in macrophages chased for 6 h after initially engulfing *E. coli* (Fig. 8, A and B, blue versus red dots in *E. coli* condition). Conversely, the fluorescence intensity associated with DQ-BSA beads was similar in cells that engulfed indigestible beads 1 h or 6 h prior during the first round of uptake, though there was a trend upward at 6 h (Fig. 8, A and B, blue versus red dots in primary

bead condition). Collectively, these observations indicate that the degradative capacity of macrophages decreases with phagocytosis and is recovered most efficiently upon phagosome resolution.

We next tested whether clathrin-mediated phagosome resolution was needed for macrophages to regain their degradative capacity. This required exposing macrophages to ikarugamycin for 6 h after phagocytosis to elicit phagosome resolution. This prolonged treatment raised concerns of potential interference with basal macrophage functions. We assessed this by measuring the degradative activity of phagosomes containing DQ-BSA beads in macrophages treated with ikarugamycin for 6 h. We found that ikarugamycin treatment did reduce phagosome proteolysis relative to vehicle (Fig. 9, A and B; no prior phagocytosis), likely due to impaired biosynthetic trafficking of proteases.

We then examined the combined effect of clathrin inhibition and prior phagocytosis. First, macrophages that engulfed *E. coli* 1 h prior had lower DQ-BSA fluorescence in subsequent phagosomes than those macrophages without a prior round of uptake (Fig. 9, A and B, blue dots for cells with no *E. coli* versus *E. coli* phagocytosis), consistent with consumption of lysosomes by the first wave of phagosomes. Second, there was an increase in DQ-BSA fluorescence in macrophages that engulfed *E. coli* 6 h prior relative to those that had engulfed *E. coli* 1 h prior (Fig. 9, A and B, blue and red dots under *E. coli* primary phagocytosis). This is consistent with results in Fig. 8. Importantly, this recovery was abolished when cells were pretreated with ikarugamycin (Fig. 9 B, green dots versus blue and red dots under *E. coli* primary phagocytosis). We then ascertained if the combined effect of clathrin inhibition and phagocytosis was greater than clathrin inhibition alone by normalizing the fluorescence of DQ-BSA beads from ikarugamycin-treated cells to vehicle-treated cells. Our data show a significant abatement in this ratio for macrophages that undertook two rounds of phagocytosis relative to

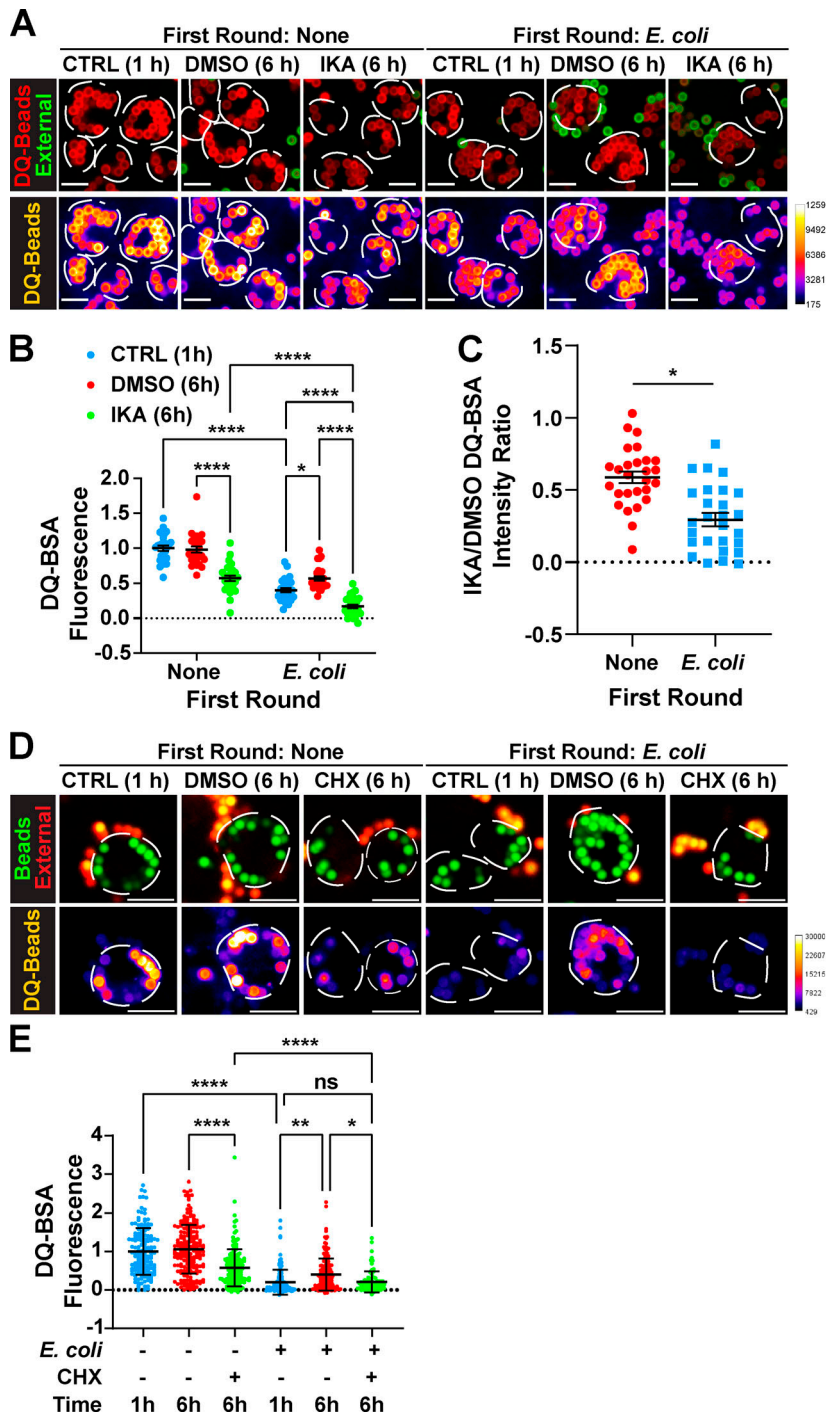


Figure 9. Clathrin-mediated phagosome resolution is required to sustain degradative capacity of macrophages. (A and D) Macrophages were given no first target or internalized *E. coli* for 1 h, followed by 1-h or 6-h chase before adding DQ-BSA-opsonized beads (red in A, green in D). Cells were treated with ikarugamycin (IKA; A), or cycloheximide (CHX; D), or vehicle (DMSO; A and D) 1 h after *E. coli* uptake. External beads were immunostained (green in A, red in D, but appear yellow) and imaged live. Lower panels show the DQ-BSA fluorescence in fire scale. Scale bars: 10 μ m. **(B and E)** Quantification of mean DQ-BSA fluorescence intensity of internalized DQ-BSA beads from experiments described in A (B) and D (E) and processed as in Fig. 8. In B, data are from 27 images across 3 independent experiments, with each image containing 1–8 cells; in E, data are based on 3 independent experiments with 82–193 cells quantified per condition. Conditions were compared statistically using a one-way ANOVA with Tukey’s test for B and two-way ANOVA with Tukey’s test for E. **(C)** Ratio of the mean fluorescence intensity of DQ-BSA in IKA- to DMSO-treated cells from data in B and shown as mean \pm SEM and compared using an unpaired *t* test (*, *P* < 0.05; **, *P* < 0.01; ****, *P* < 0.0001).

those that engulfed only DQ-BSA beads (Fig. 9 C). Finally, we postulated that the biosynthetic pathway may aid in maintaining the degradative capacity of macrophages during phagosome resolution. First, we observed that cycloheximide did not impair phagosome fragmentation, suggesting that the first wave of phagosomes had sufficient hydrolytic enzymes to complete digestion and resolution (Fig. S4, A and B). However, there was a reduction in phagosome-associated proteolytic activity in cells treated with cycloheximide with or without a prior round of phagocytosis (Fig. 9, D and E). Overall, phagosome resolution coupled to biosynthesis is important to recycle lysosomes and

maintain degradative proficiency of macrophages to handle subsequent rounds of phagocytosis.

Discussion

For every phagosome formed, membrane resources, including plasma membrane, endosomes, and lysosomes, are consumed, and thus membrane resynthesis and retrieval are critical to keep phagocytes functional (Zent and Elliott, 2017). Yet, how phagocytes balance cellular resources is largely uncharacterized, though synthesis of plasma membrane lipids has been observed

(Werb and Cohn, 1972). Here, we show that macrophages predominantly resolve phagosomes via fragmentation rather than through egestion. This fission process leans on particle degradation, the cytoskeleton, and clathrin. Moreover, we present evidence that phagolysosome resolution is critical in restoring lysosomes that have been consumed during phagosome maturation and to sustain proteolytic activity in macrophages that ceaselessly iterate phagocytosis, with the biosynthetic pathway likely supplying new hydrolytic enzymes.

The ultimate fate of phagolysosomes

Phagolysosome exocytosis was assumed to expel indigestible material and return membrane to the surface of phagocytes (Stewart and Weisman, 1972; Maniak, 2003; Clarke et al., 2002; Gotthardt et al., 2002). Yet, we failed to observe exocytosis of phagosomes containing either bacteria or beads. Instead, smaller PDVs formed, coupled to the disappearance of recognizable phagosomes. This phagosome fragmentation proceeded through splitting, tubulation, and budding, suggesting at least three distinct mechanisms. This aligns with previous observations showing that efferosomes and phagosomes containing RBCs shrink or fragment into phagosome-derived membrane compartments (Krajcovic et al., 2013; Levin-Konigsberg et al., 2019; Poirier et al., 2020). Collectively, these observations suggest that phagosome resolution is typically driven by fragmentation using distinct mechanisms of membrane fission rather than exocytosis, irrespective of the nature of the cargo. Yet, we have not excluded exocytosis as a mechanism of phagosome resolution for all modes of phagocytosis, such as the uptake of indigestible particulates captured by alveolar macrophages or resolution of phagosomes with pathogenic microorganisms (Ma et al., 2006; Alvarez and Casadevall, 2006). Moreover, some phagosome-derived cargo may eventually undergo secretion as detected by cleaved bacteria-derived mRFP1 in the media of phagocytes after phagocytosis; this may occur through direct PDV secretion or indirectly through exchange with preexisting compartments.

In addition, while tubulation, budding, and splitting are detectable during phagosome resolution, it is important to state that membrane fission occurs throughout the lifetime of the phagosome, not simply during resolution (Saffi and Botelho, 2019). For example, COPI-mediated fission occurs on phagosomes to extract the transferrin receptor from early phagosomes (Botelho et al., 2000a), while the cytoskeleton mediates recycling from phagosomes enclosing latex beads (Damiani and Colombo, 2003). Moreover, major histocompatibility complex class II:peptide complexes exit phagosomes likely before resolution ensues, though the exact mechanism and timing are unclear (Harding and Geuze, 1992; Mantegazza et al., 2013, 2014; Ramachandra et al., 1999). Finally, tubules can dynamically form between phagosomes to exchange phagosomal content with implications for antigen presentation (Mantegazza et al., 2014). All these processes occur before phagosomes become unidentifiable as such. Thus, we propose a model in which membrane fission happens throughout the lifetime of the phagosome, where early maturation and midmaturation serve to sort and remove cargo from the phagosome without its disintegration, whereas end-of-life fission culminates in phagosome disappearance. It will

be exciting to define if these represent distinct fission complexes or common fission assemblies that are regulated differently during the lifespan of the phagosome.

Cargo degradation in phagolysosome resolution

Through inhibition of lysosomal proteases and neutralization of the phagosomal pH, we provide evidence that cargo degradation is required for phagosomal resolution. Mechanistically, we envision two nonmutually exclusive possibilities for this requirement. First, loss of physical integrity by cargo degradation may be a *sine qua non* for phagosome fission. Supporting this concept, undegradable large latex beads remain enclosed within phagosomes for prolonged periods of time. On the other hand, IgG-agglutinated nanobead clusters fragment through degradation and disaggregation of IgG, which allows phagosomal fragmentation. Second, digestible cargo, like bacteria, contains a complex mix of macromolecules that are degraded to release monomers, like amino acids, that become available for use within the phagocyte. This bolus of amino acids may be sensed by intraluminal or cytoplasmic amino acid sensors that locally promote mTORC1 activation (Saxton et al., 2016; Chantranupong et al., 2016; Zoncu et al., 2011; Inpanathan and Botelho, 2019). While mTORC1 drives many anabolic processes, like protein and lipid synthesis, mTORC1 also plays a role in coordinating phagosome and lysosome dynamics, including efferosome fission (Krajcovic et al., 2013; Inpanathan and Botelho, 2019; Saric et al., 2016; Hipolito et al., 2019). Thus, cargo degradation coupled to mTORC1 activation could help orchestrate phagosome resolution. This would parallel the role of mTORC1 reactivation during the degradation of autophagic cargo to regenerate lysosomes (Yu et al., 2010).

Requirements for phagosome resolution

We observed that drugs that stabilized or depolymerized the actin and microtubule cytoskeletons, as well as inhibitors of clathrin and dynamin, all impaired phagosome fragmentation. These, together with our observations that phagosomes split, tubulate, and bud, imply that phagosome resolution ensues through multiple mechanisms. For example, actin may play a role in membrane constriction via actomyosin complexes that could distort phagosomes (Liebl and Griffiths, 2009; Curchoe and Manor, 2017; Poirier et al., 2020). Alternatively, short branched actin assemblies are associated with fission of endosomes/lysosomes through contacts with the ER (Rowland et al., 2014; Hoyer et al., 2018). On the other hand, microtubules may aid in resolution via membrane tubulation and extrusion, as they do during early phagosome tubulation, autophagic lysosome reformation, and endosome tubulation (Du et al., 2016; Delevoye et al., 2014; Harrison et al., 2003). This likely depends on the combined action of dynein and kinesin motor proteins modulated by Rab7 and/or Arl8b GTPases (Jordens et al., 2001; Garg et al., 2011). However, a challenge in assessing the role of these proteins in phagosome resolution is that they are also required for maturation, and hence altering their function will interfere with both phases of the pathway (Harrison et al., 2003; Garg et al., 2011). The development of tools that can deactivate these proteins acutely is necessary to dissect their roles in phagosome maturation versus resolution.

Finally, by using independent compounds, like ikarugamycin, Pitstop, dynole 34-2, and dyngo-4a, and induced chemical displacement of clathrin, we found that clathrin and possibly dynamin are required for budding events at the phagolysosome. The role of clathrin on lysosomes remains poorly defined, despite early observations that clathrin associates with lysosomes and that multiple adaptor protein complexes act on lysosomes or lysosome-like organelles (Arneson et al., 1999; Traub et al., 1996; Saffi and Botelho, 2019). More recently, clathrin and adaptor protein complexes like AP-2 were discovered to have a role in lysosome regeneration from spent autolysosomes. This requires the recruitment of distinct PIPKI isoforms to spent autolysosomes to generate a first burst of phosphatidylinositol 3,5-bisphosphate that leads to assembly of clathrin to nucleate a tubule, followed by a second burst at the tips of the tubules that helps induce clathrin-mediated vesiculation of lysosome precursors (Rong et al., 2012). Whether a similar process occurs on resolving phagosomes is unknown. Ultimately, the initiation and coordination of phagosome resolution may depend on the type of phagosomal cargo, its physical parameters like particle rigidity, and catabolites generated during degradation, which may interface with mTOR, the actomyosin cytoskeleton, and the membrane curvature machinery.

Lysosome consumption and regeneration during phagosome resolution

We provide evidence that phagosome maturation consumes free lysosomes, limiting the degradative capacity of subsequently formed phagosomes. However, we also observed that this is a transient phenomenon since cells with “degradable” phagosomes recovered free lysosomes and subsequent phagosomes had higher proteolytic activity than cells that engulfed indigestible cargo or whose earlier phagosomes did not “resolve.”

Importantly, clathrin inhibition impaired phagosome resolution and prevented subsequent phagosomes from acquiring their full degradative potential relative to control conditions. Admittedly, prolonged clathrin inhibition is a complex manipulation likely to have indirect effects. Indeed, clathrin inhibitors alone caused a reduction in the degradative capacity of phagosomes, likely by impairing trafficking of newly synthesized hydrolases (Le Borgne and Hoflack, 1997; Ludwig et al., 1994). This is consistent with reduced degradation of phagosomes formed after an initial round and in cells treated with cycloheximide. Nevertheless, the combined effect of clathrin inhibition and phagosomal load greatly hindered the proteolytic activity of subsequent phagosomes. This suggests that failure to undergo resolution of earlier phagosomes reduced the capacity of macrophages to deal with subsequent rounds of phagocytosis.

Overall, we propose that phagosome resolution helps regenerate lysosomes consumed during phagosome maturation. Yet, we suspect that PDVs are heterogeneous and may consist of distinct lysosome-like intermediates. Given that 80% of PDVs possessed lysosomal proteins and an acidic and proteolytic lumen, we speculate that phagosome resolution mostly regenerates endolysosome-like compartments (Bright et al., 2005). Yet, a fraction of PDVs may be akin to terminal storage

lysosomes (Bright et al., 2005) or protolysosomes, which are depleted of degradative capacity as observed during autophagic lysosome reformation (Yu et al., 2010). Additionally, we suspect that the biosynthetic pathway and transcription factor EB-mediated activation may play a role in maintaining the degradative power of subsequent phagosomes (Gray et al., 2016). Thus, we propose dedicated studies to better dissect the relative contributions of phagosome resolution, lysosome reformation, and biosynthetic pathways toward maintaining macrophage degradative power after phagocytosis.

Materials and methods

Cell culture, transfection, and mammalian

expression constructs

RAW 264.7 murine macrophages (ATCC TIB-71; American Type Culture Collection) were cultured at 37°C and 5% CO₂ in DMEM supplemented with 10% heat-inactivated FBS (Wisent Inc.). The CLC-GFP construct was a gift from Dr. C. Antonescu (Ryerson University, Toronto, Ontario, Canada) and was described by Aguet et al. (2013). The construct encoding PLCδ-PH-GFP was from Addgene and was described by Stauffer et al. (1998). pMito-mCherry-FRB (MitoTrap) and GFP-FKBP-CLCa are plasmid constructs used for rapamycin-induced clathrin displacement (clathrin knocksideways) were kindly provided by S. Royle (University of Warwick, Coventry, UK) and were described by Cheeseman et al. (2013). Macrophages were transfected using FuGENE HD (Promega) according to the manufacturer’s instructions.

Bone marrow–derived primary macrophage (BMDM) culture

BMDMs were harvested from WT 7–9-wk-old female C57BL/6 mice. Briefly, bone marrow was perfused from femurs and tibias with PBS using a 27-gauge syringe. RBCs were eliminated by osmotic lysis, and BMDMs were differentiated in DMEM supplemented with 10% heat-inactivated FBS, 20 ng/ml recombinant mouse macrophage colony-stimulating factor (PeproTech), and 5% penicillin/streptomycin (Sigma-Aldrich). Cells were incubated at 37°C with 5% CO₂. The medium was changed every 2 d. Experiments were conducted on day 7 of bone marrow isolation. All animals were used following institutional ethics requirements.

Preparation of bacterial targets

To obtain fluorescently labeled *E. coli*, the DH5α *E. coli* strain was transformed with the pBAD::mRFP1 plasmid (Addgene, plasmid 54667; Campbell et al., 2002) or the pZsGreen vector (catalog no. 632446; Takara Bio USA, Inc.). Transformed *E. coli* were grown overnight at 37°C on Luria-Bertani (LB) agar plates, and colonies were subsequently cultured overnight at 37°C in LB broth under agitation. The agarized and broth media were supplemented with 100 μg/ml ampicillin (BioShop Canada Inc.). For ZsGreen-*E. coli*, 1% D-glucose (BioShop) was also added to the LB plates and broth to suppress leaky expression of ZsGreen from the *lac* operon. The overnight cultures were subcultured at 1:100 dilution and grown at 37°C until midlog phase, at which time mRFP1 expression was induced through supplementation with

5 mM L-arabinose (BioShop) for 4 h, while ZsGreen expression was induced with 1 mM IPTG (Sigma-Aldrich) for 3 h. *E. coli* bacteria were subsequently fixed in 4% PFA (Electron Microscopy Sciences) in PBS.

To obtain fluorescently labeled filamentous targets, mCherry-*Lp* was prepared as described previously (Prashar et al., 2013). Briefly, *Lp* containing the KB288 plasmid, a gift from Dr. A.K. Brassinga (University of Manitoba, Winnipeg, Manitoba, Canada) and described in Brassinga et al. (2010), were first grown at 37°C and 5% CO₂ on buffered charcoal-yeast extract plates for 3 d. Colonies were grown for an additional 24 h at 37°C in buffered yeast extract media under agitation. The *Lp* filaments were then killed with 4% PFA solution. For the analysis of phagosome resolution using filaments, bacteria longer than 15 μm were considered filamentous (Prashar et al., 2013).

Phagocytosis assays

For the phagocytosis of *Lp* filaments, the PFA-killed bacteria were opsonized with 0.1 mg/ml of rabbit anti-*Legionella* antibody (Public Health Ontario) for 1 h at RT (Prashar et al., 2013). RAW macrophages were pre-cooled to 15°C for 5 min before cells were challenged with filaments at a ratio of 150 filaments per macrophage. Bacterial attachment was synchronized by spinning the cells at 300 × *g* for 5 min at 15°C. Following a 15-min incubation at 37°C, unbound filaments were washed off with PBS. Macrophages were subsequently incubated at 37°C to allow phagocytosis to progress to the indicated time points, at which time the cells were either fixed with 4% PFA for 20 min or imaged live.

For the phagocytosis of *E. coli* rods and beads, the bacteria, 3.87-μm polystyrene latex beads (Bangs Laboratories), or 3.0-μm polystyrene latex beads (Sigma-Aldrich) were opsonized with 4 mg/ml of human IgG (I8640 or I4506; Sigma-Aldrich) for 1 h at RT. To coat beads with DQ-BSA, a 5% wt/vol suspension of 3.0-μm beads or 0.5% wt/vol suspension of 2.0-μm Dragon Green fluorescent beads (Bangs Laboratories) was incubated with 0.5 mg/ml DQ-Red BSA (Thermo Fisher Scientific) for 1 h before opsonization with human IgG or 200 μg/ml rabbit anti-BSA antibody (LSA11133; Fisher Scientific). RAW cells were pre-cooled to 4°C for 5 min before the cells being presented with targets at ratios of 20–400 rods per cell, 10 3.87-μm beads per cell, or 25–135 3.0-μm beads per cell, depending on if phagosomal saturation was required. Target attachment was synchronized by spinning cells at 300 × *g* for 5 min at 4°C. Following a 15–60-min incubation at 37°C, unbound targets were washed off with PBS. The cells were then incubated at 37°C to allow phagocytosis to progress to the indicated time points and either fixed with PFA or imaged live. For assays using two rounds of phagocytosis, the procedure for both the first and second rounds of phagocytosis was the same as described above, except the secondary phagocytic challenge was done after the first round of phagocytosis at specified times. The secondary challenge was then followed with no chase or 1-h chase to elicit further maturation before fixation or live-cell imaging.

For the phagocytosis of bead clumps, 0.1-μm TetraSpeck microspheres (blue/green/orange/dark red; Thermo Fisher

Scientific) were opsonized with 4 mg/ml of human IgG for 1 h at RT before leaving the mixture at 4°C overnight. Macrophages were pre-cooled to 4°C for 5 min before the cells were presented with bead clumps at ratios of 1,400 beads per cell. Bead clumps were spun onto the cells at 300 × *g* for 5 min at 4°C. Following a 15-min incubation at 37°C, unbound bead clumps were washed off with PBS. Macrophages were subsequently incubated at 37°C to allow phagocytosis to progress to the indicated time points, at which point the cells were imaged live.

Exocytosis of phagosomal content

Following phagocytosis of mRFP1-labeled *E. coli* and incubation for 1 h, 6 h, and 24 h, the cell media were centrifuged at 10,000 × *g* for 3 min to remove loose bacteria and cellular debris. To assess mRFP1 in the cell-free supernatant, proteins were precipitated using ice-cold TCA (BioShop) added to a final concentration of 10%. The mixture was incubated on ice for 20 min at RT and centrifuged at 17,000 × *g* for 2 min. The TCA precipitate was washed twice with ice-cold acetone (BioShop), resuspended by sonication, and centrifuged at 17,000 × *g* for 2 min. Pellets were dried and then resuspended in 1× Laemmli buffer.

To assess mRFP1 in phagosomes, cells were washed three times with ice-cold PBS treated to remove bacteria adhered to the cells. Cells were then washed three times with ice-cold PBS and lysed with 1× Laemmli buffer. 50 μl of mRFP1-labeled *E. coli* at 1 OD was also lysed with 1× Laemmli buffer.

The contents of the *E. coli*, sample media, and cells were analyzed by Western blotting. Cell lysates and media precipitates were resolved on a 15% SDS-PAGE gel and transferred onto polyvinylidene difluoride membranes. Membranes were blocked with 5% BSA in TBS containing 0.1% Tween-20 (TBST) for 1 h at RT, then labeled overnight at 4°C with rabbit anti-RFP antibody (1:1,000, 600-401-379-RTU; Rockland Immunochemicals, Inc.) or rabbit anti-GAPDH antibody (1:1,000, 2118S; Cell Signaling Technology); primary antibodies were diluted in 1% BSA with TBST. HRP-conjugated donkey anti-rabbit antibodies (Bethyl Laboratories) were used at 1:10,000 in 1% BSA with TBST for 3 h at RT. Membranes were washed three times with TBST for 5 min each wash and developed with Clarity Western ECL Substrate (Bio-Rad Laboratories). Western blot bands were visualized using the ChemiDoc Touch Imaging System (Bio-Rad Laboratories). Blot images were analyzed by ImageLab (Bio-Rad Laboratories). The background was automatically determined and subtracted from each band by the software, which employed a rolling disk method with a disk size of 10 mm to determine the background intensities along the lane. The background values corresponding to the positions of the bands were used to subtract the background from the respective bands. mRFP1 from phagolysosomes was identified by the increased gel migration compared with native mRFP1 (Katayama et al., 2008). Cleaved mRFP1 volume was normalized to GAPDH volume.

Isolation of phagosomes

To isolate phagosomes, a sucrose gradient was prepared by adding 1 ml of 60% sucrose suspension to a 1-ml ultracentrifuge tube, and the solution was centrifuged at 50,000 × *g* for 1 h at

4°C. Following centrifugation, the sucrose gradient was carefully placed on ice until use. Macrophages were allowed to internalize IgG-opsonized polystyrene beads for 60 min. Following phagocytosis, the cell media were replaced with cold homogenization buffer (20 mM Tris; BioShop), 1:400 protease inhibitor cocktail (Sigma-Aldrich), 1 mM 4-(2-aminoethyl)-benzenesulfonyl fluoride (BioShop), 1 mM MgCl₂ (Thermo Fisher Scientific), 1 mM CaCl₂ (Biobasic), 0.02 mg/ml RNase (Roche Diagnostics), and 0.02 mg/ml DNase (Roche), pH 7.4, and the cells were dislodged by mechanical scraping. The cell suspension was centrifuged at 500 × *g* for 5 min at 4°C, and the pellet was resuspended in homogenization buffer. Cells were lysed by passing the suspension through a 22-gauge needle 5–10 times, then the lysate was centrifuged at 1,000 × *g* for 5 min. The pellet was resuspended in 4% PFA and incubated at RT for 20 min to fix the lysate and secure protein complexes on the phagosome surface. The pellet was washed three times with PBS followed by centrifugation at 3,000 × *g* for 5 min per wash, then resuspended in 200 μl PBS. To separate phagosomes from the resuspended lysate pellet, the resuspended pellet was loaded onto the sucrose gradient and then centrifuged at 21,000 × *g* for 10 min at 4°C. The bead-containing fraction was extracted from the gradient with a 22-gauge needle and washed with ice-cold PBS.

Pharmacological inhibitors

Inhibitors and the DMSO (BioShop) vehicle control were applied after phagocytosis and maintained until fixation or the conclusion of the experiment. To increase cytosolic Ca²⁺, cells were incubated with 10 μM of ionomycin (Sigma-Aldrich) and 1.2 mM of CaCl₂ (BioShop) 1–2 h after phagocytosis for up to 1 h. For pH neutralization of the phagolysosome, macrophages were treated with 1 μM Con A (BioShop) and 10 mM NH₄Cl (BioShop) 40 min after the start of phagocytosis. To inhibit proteases, cells were incubated with a protease inhibitor cocktail (Sigma-Aldrich) 40 min after phagocytosis, which included 1.0 mM 4-(2-aminoethyl)-benzenesulfonyl fluoride, 0.8 μM aprotinin, 40.0 μM bestatin, 14.0 μM E-64, 20.0 μM leupeptin, and 15.0 μM pepstatin A. To inhibit the cytoskeleton and dynamin, macrophages were treated with the following inhibitors 40 min after phagocytosis: 10 μM nocodazole (Sigma-Aldrich), 10 μM Taxol (Sigma-Aldrich), 2 μM cytochalasin D (EMD Millipore), 1 μM jasplakinolide (EMD Millipore), 5 μM dyngo-4a (Abcam), and 5 μM dynole 34-2 (Abcam). For clathrin inhibitors, cells were incubated with 10 μM of Pitstop 2 (Abcam) or 0.5–2.0 μg/ml ikarugamycin (Sigma-Aldrich) 40 min to 4 h after the start of phagocytosis. To inhibit de novo protein synthesis, macrophages were treated with 1 μM cycloheximide (BioShop) 1 h after phagocytosis.

Rapamycin-induced clathrin displacement (clathrin knocksideways)

After 24 h of transfection, cells were treated with 1 μM rapamycin (BioShop) or DMSO for 1 h. After 1 h, 0.5 OD of nonlabeled *E. coli* was added to each well with or without rapamycin and pulsed for 30 min at 37°C and 5% CO₂. Cells were washed three times with 1× PBS, and warm medium was added and chased for 3 h. For staining internalized *E. coli*, PFA-fixed cells were permeabilized with 0.1% Triton X-100 for 20 min at RT. Cells

were washed three times with 1× PBS and incubated at RT with 1:100 rabbit anti-*E. coli* antibody (Bio-Rad Laboratories) prepared with 1% BSA. Cells were washed with 1× PBS three times and incubated with 1:1,000 fluorescent donkey-derived secondary antibody in 1% BSA for 1 h at RT. After the last wash, coverslips were mounted using Dako mounting medium and imaged. The number of fragments in control and rapamycin-treated cells was counted using ImageJ.

Immunofluorescence and fluorescence labeling

External beads were stained for live-cell imaging by incubating macrophages with Cy2-conjugated donkey anti-human IgG (1:100 in PBS; Jackson ImmunoResearch Laboratories) for 30 min on ice. For internal staining, PFA-fixed cells were permeabilized with 0.1% Triton X-100 for 20 min with the exception of staining with the LAMP1 antibody, which required permeabilization with ice-cold methanol for 5 min instead. Primary antibodies that were diluted in 5% skim milk or 1% BSA solution were applied for 1 h at RT and included rabbit anti-*Legionella* antibody (1:3,000; Public Health Ontario), rabbit anti-*E. coli* antibody (1:100; Bio-Rad Laboratories), rat anti-LAMP1 antibody (1:200, 1D4B; Developmental Studies Hybridoma Bank), and rat anti-LAMP2 antibody (1:100, ABL-93; Developmental Studies Hybridoma Bank). Fluorescent secondary donkey antibodies (Thermo Fisher Scientific or Bethyl Laboratories) were used at a 1:1,000 dilution in 5% skim milk or 1% BSA solution for 1 h at RT. The coverslips were mounted using Dako fluorescence mounting medium (Agilent Technologies, Inc.).

For labeling acidic compartments, cells were stained with LysoTracker Red DND-99 at 1 μM for 1 h (Thermo Fisher Scientific). To label degradative compartments, cells were labeled with Magic Red Cathepsin-L substrate (ImmunoChemistry Technologies) for 1 h, as per the manufacturer's instructions.

For labeling isolated phagosomes, phagosomes were incubated with the following primary antibodies: anti-LAMP1 (1:200 in PBS) and rabbit anti-clathrin heavy chain (1:200 in PBS; D3C6). Phagosomes were washed three times with 0.5% BSA followed by centrifugation at 2,000 × *g* for 1 min. Fluorescent secondary donkey antibodies were added to the phagosomes at a 1:1,000 dilution and incubated for 1 h at RT, then phagosomes were washed three times with 0.5% BSA followed by centrifugation at 2,000 × *g* for 1 min. Phagosomes were resuspended in PBS and mounted with Dako mounting medium.

Microscopy

Confocal images were acquired using two different spinning-disk confocal microscope systems. The first was a Quorum Wave FX-X1 spinning-disk confocal microscope system (Quorum Technologies, Inc.) consisting of an inverted fluorescence microscope (DMI6000B; Leica Microsystems) equipped with a Hamamatsu ORCA-R² camera (C10600-10B) and a Hamamatsu ImagEM Enhanced EM charge-coupled device (CCD) camera (Hamamatsu Corporation). The second was a Quorum Diskovery spinning-disk confocal microscope system (Quorum Technologies, Inc.) consisting of an inverted fluorescence microscope (DMI8; Leica) equipped with the Andor Zyla 4.2-megapixel

scientific complementary metal-oxide-semiconductor and Andor iXON 897 EM-CCD camera (Oxford Instruments). We also used an inverted microscope (IX81; Olympus Life Science) equipped with a Rolera-MGI Plus EM-CCD camera (ROL-MGI-PLUS-F-M-14-C; Q Imaging). The microscope systems were controlled by MetaMorph acquisition software (Molecular Devices). Images were acquired using a 63× oil immersion objective (1.4 NA), a 40× oil immersion objective (1.3 NA), or a 40× dry objective (0.60 NA). For fixed-cell imaging, Dako-mounted coverslips were imaged at RT. For live-cell imaging, coverslips were imaged in a chamber containing DMEM supplemented with 10% FBS in a microscope-mounted chamber maintained at 37°C and 5% CO₂.

Live-cell imaging of clathrin-GFP and phagosome resolution

1 d after transfection of clathrin-GFP, RAW cells were given mRFP1-expressing *E. coli* bacteria to engulf. After 30 min, the bacteria in the media were removed by washing the cells three times with PBS, and warm culture media were added to allow phagocytosis maturation for 1–2 h. Live-cell imaging was performed, keeping cells at 5% CO₂ and 37°C in an environmental control chamber with a Quorum Diskovery spinning-disk confocal microscope set to acquire a five-plane z-stack at 0.4- μm intervals at 1 frame/5 s for 5-min periods. Imaging analysis was done with ImageJ (National Institutes of Health) by counting the number of clathrin-positive and clathrin-negative fission events (tubule formation, budding, constriction).

Image processing and analysis

Image processing and quantitative analysis were performed using Fiji (Schindelin et al., 2012) or Volocity (PerkinElmer), where image enhancements were completed without altering the quantitative relationship between image elements. For the quantification of the total volume of *E. coli*-containing phagosomes in each cell, phagosomes were first identified in Volocity by their high fluorescence intensity and then by their volume, set as $>1 \mu\text{m}^3$. The volumes of phagosomes in each cell were added together for each time point and normalized to the first acquisition time point (T_0). For the quantification of the total volume of PDVs containing *E. coli*-derived debris, we had Volocity select dimmer fluorescence objects and then defined their volume as $>0.02 \mu\text{m}^3$ but $<5 \mu\text{m}^3$. The volumes of individual PDVs in each cell were summed and, in the case of time-lapse microscopy, normalized to the first time point. Phagosomes were excluded from the PDV quantifications because the inclusion of lower fluorescence intensities allowed PDVs closely surrounding the phagosome to be included within the phagosome volume, thereby increasing the apparent size of the phagosomes above the volume threshold for PDVs (Fig. S5). For the quantification of the total volume of *Lp*-containing phagosomes and PDVs in each cell, we used the same methodology as for *E. coli*, except that the phagosomes were included in the quantifications if their volume exceeded $5 \mu\text{m}^3$. For the co-occurrence of LysoTracker Red or Magic red with PDVs containing *E. coli*-derived debris, we used Manders colocalization analysis in Volocity, where PDVs were included within this analysis if their surface area was $>0.1 \mu\text{m}^2$ but $<4 \mu\text{m}^2$. The

markers were considered to co-occur when the M_2 colocalization coefficient was determined to be >0.7 . We then reported the percentage of PDVs that were positive for Magic red or LysoTracker Red (co-occurrence of markers).

For the counting of phagosome and PDV events, images of mRFP1-labeled *E. coli* and PDVs were first thresholded to exclude background and macrophage autofluorescence signals and to minimize signal overlap of events while retaining as much of the low-intensity events as possible. Once an intensity threshold was identified, it was applied to all images of all samples of the same experimental replicate. External events were identified by colocalization with external anti-*E. coli* fluorescence signal and excluded from analysis. The thresholded images were used to create binary images of the samples, and the binary images were processed by object segmentation using Fiji's Watershed function. Intact phagosome events were identified manually by the rod-shaped events characteristic of *E. coli*'s shape. PDVs between $0.015 \mu\text{m}^2$ and $1.2 \mu\text{m}^2$ were counted using Fiji's Analyze Particles function.

For the quantification of the number of free lysosomes in each cell, we used Volocity to separate touching objects in the LAMP1 channel using an object size guide of $0.29 \mu\text{m}^3$ (determined by assessing the lysosome size in resting macrophages). LAMP1-positive objects were considered free lysosomes if their volume was $>0.02 \mu\text{m}^3$ but $<5 \mu\text{m}^3$ and they were not touching the filament-containing phagolysosomes (applied a mask to the filament). The treatments were finally normalized to the no-phagocytosis group, which was considered to contain 100% free lysosomes.

For the determination of the presence or absence of LAMP1 and LAMP2 on PDVs, first, PDVs in an image were identified as vesicles with an image area between $0.015 \mu\text{m}^2$ and $1.2 \mu\text{m}^2$. Then PDVs were assessed for the presence or absence of LAMP1 or LAMP2 colocalized to the PDV, and cells were scored by the percentage of PDVs with colocalized LAMP1 or LAMP2 fluorescence signal.

For the determination of phagosome mixing, images of second-wave phagosomes (GFP) and fragments were thresholded to exclude background and macrophage autofluorescence signals, then a binary mask was formed. Second-wave events external to the cell were determined by comparison to bright-field images and excluded from the mask. The mean fluorescence intensity of first-wave phagosome remnants (mRFP1) colocalized to the second-wave mask was determined and corrected by numerical subtraction of mean background intensity. For the determination of the percentage of beads positive for *Legionella* fragments, beads were manually scored and considered positive if bacterial debris was observed to completely surround the bead. For the determination of DQ-BSA intensity, images in a stack corresponding to the lower half of DQ-BSA beads were collapsed by maximum-intensity projection (MIP), and the MIP images were thresholded to exclude non-DQ-BSA bead events. External beads were identified by colocalization of Cy2 anti-human or Cy3 anti-human fluorescent signal and excluded from analysis by relevant mask subtraction. Following mask subtraction, DQ-BSA proteolytic activity was determined by measuring the mean fluorescence of internalized beads and

corrected by numerical subtraction of mean external DQ-BSA bead intensity. Because there are multiple sources of heterogeneity (uptake of first-round particles, age and resolution of phagosomes, uptake of second-round phagosomes, age of second-round phagosomes, and level of DQ-BSA labeling of beads), we analyzed the entire sampled population rather than the sampled mean. Deconvolution (30 iterations) was performed using Volocity software. Figures were assembled using Adobe Illustrator (Adobe Systems, Inc.).

Statistical analysis

Unless otherwise indicated, data are presented as the mean \pm SEM of at least three independent experiments. The number of cells assessed in each experiment is indicated within the figure legends. Statistical analysis was performed using GraphPad Prism software (GraphPad Software, Inc.). Unless otherwise indicated, data were assumed to be normally distributed but were not formally tested; additionally, an unpaired, two-tailed Student's *t* test was used to compare two conditions, while multiple conditions were compared using one-way ANOVA with Tukey's post hoc test, two-way ANOVA with Tukey's post hoc test, or two-way ANOVA with Sidak's post hoc test. Curves were fit to the data using nonlinear regression, where Akaike Information Criterion was used to select the model that best fit the data. The coefficient of determination (R^2) was determined for the quadratic function fit to the phagosome data and the exponential function fit to the PDV data. The slopes of the lines using linear regression were statistically compared using analysis of covariance. In any of the statistical tests performed, $P < 0.05$ was considered significant.

Online supplemental material

Fig. S1 is complementary to **Fig. 1** and shows that phagosomes do not undergo exocytosis even in the presence of ionomycin, that phagosomes can fragment even if the cargo is indigestible, and that degraded phagosomal content can be secreted. **Fig. S2** is complementary to **Figs. 4** and **5** and shows that clathrin associates with bead-containing phagosomes, that clathrin inhibitors reduce the number of PDVs in fixed RAW cells, and that clathrin inhibitors block phagosome resolution at earlier time points of phagosome resolution and in primary mouse macrophages. **Fig. S3** is complementary to **Fig. 5** and shows that dynamin inhibitors block phagosome resolution. **Fig. S4** is complementary to **Fig. 9** and shows that cycloheximide treatment after phagocytosis was insufficient to arrest phagosome fragmentation. **Fig. S5** outlines the method in which the total volume of fragments was determined using image analysis. **Video 1** is complementary to **Fig. 1** and shows that internalized beads remain within RAW cells over a 24-h period. **Video 2** is complementary to **Fig. 1** and shows a time lapse of a *Legionella*-containing phagosome undergoing fragmentation. **Video 3** is also complementary to **Fig. 1** and shows a time lapse of *E. coli*-containing phagosomes undergoing fragmentation. **Video 4** is complementary to **Fig. S1** and shows a time lapse of phagosomes containing aggregated fluorescent nanobeads undergoing fragmentation. **Video 5** is complementary to **Fig. 3** and illustrates a time lapse of an early budding event occurring on a phagosome with a mostly intact cargo. **Video 6** is complementary to **Fig. 3** and displays a time lapse of a late

budding event occurring on a phagosome with degraded cargo. **Video 7** is complementary to **Fig. 3** and shows a time lapse of a tubulation event occurring on a phagosome. **Video 8** is complementary to **Fig. 3** and exhibits a time lapse of a phagosome splitting into two pieces. **Video 9** is complementary to **Fig. 4** and shows that clathrin is associated with phagosomes and phagosome fission sites. **Video 10** is complementary to **Fig. 5** and illustrates that inhibition of clathrin with Pitstop prevents fragmentation of *Legionella*-containing phagosomes.

Acknowledgments

The rabbit anti-*Legionella* antibodies were a kind gift from Public Health Ontario (Toronto, Ontario, Canada).

This work was funded by the Natural Sciences and Engineering Council of Canada (RGPIN-2018-05734 and RGPAS-2018-522692) to M.R. Terebiznik and R.J. Botelho and by the Canadian Institutes of Health Research (123373), the Canada Research Chairs program, the Early Researcher Award from the Government of Ontario (ER13-09-042), and Ryerson University to R.J. Botelho.

The authors declare no competing financial interests.

Author contributions: C.E. Lancaster, A. Fountain, R.M. Dayam, M.R. Terebiznik, and R.J. Botelho designed the concepts, project, and experiments. C.E. Lancaster, A. Fountain, R.M. Dayam, E. Somerville, J. Sheth, A. Somerville, and V. Jacobelli performed experiments and analyzed and interpreted data. M.R. Terebiznik and R.J. Botelho secured funding and managed progression of the project. C.E. Lancaster, A. Fountain, M.R. Terebiznik, and R.J. Botelho wrote and edited the paper and generated figures.

Submitted: 14 May 2020

Revised: 5 May 2021

Accepted: 14 June 2021

References

- Aguet, F., C.N. Antonescu, M. Mettlen, S.L. Schmid, and G. Danuser. 2013. Advances in analysis of low signal-to-noise images link dynamin and AP2 to the functions of an endocytic checkpoint. *Dev. Cell.* 26:279–291. <https://doi.org/10.1016/j.devcel.2013.06.019>
- Alvarez, M., and A. Casadevall. 2006. Phagosome extrusion and host-cell survival after *Cryptococcus neoformans* phagocytosis by macrophages. *Curr. Biol.* 16:2161–2165. <https://doi.org/10.1016/j.cub.2006.09.061>
- Arneson, L.S., J. Kunz, R.A. Anderson, and L.M. Traub. 1999. Coupled inositolide phosphorylation and phospholipase D activation initiates clathrin-coat assembly on lysosomes. *J. Biol. Chem.* 274:17794–17805. <https://doi.org/10.1074/jbc.274.25.17794>
- Bezanilla, M., A.S. Gladfelter, D.R. Kovar, and W.-L. Lee. 2015. Cytoskeletal dynamics: a view from the membrane. *J. Cell Biol.* 209:329–337. <https://doi.org/10.1083/jcb.201502062>
- Bissig, C., I. Hurbain, G. Raposo, and G. van Niel. 2017. PIKfyve activity regulates reformation of terminal storage lysosomes from endolysosomes. *Traffic.* 18:747–757. <https://doi.org/10.1111/tra.12525>
- Botelho, R.J., D.J. Hackam, A.D. Schreiber, and S. Grinstein. 2000a. Role of COPI in phagosome maturation. *J. Biol. Chem.* 275:15717–15727. <https://doi.org/10.1074/jbc.M910068199>
- Botelho, R.J., M. Teruel, R. Dierckman, R. Anderson, A. Wells, J.D. York, T. Meyer, and S. Grinstein. 2000b. Localized biphasic changes in phosphatidylinositol-4,5-bisphosphate at sites of phagocytosis. *J. Cell Biol.* 151:1353–1368. <https://doi.org/10.1083/jcb.151.7.1353>

- Brassinga, A.K.C., J.M. Kinchen, M.E. Cupp, S.R. Day, P.S. Hoffman, and C.D. Sifri. 2010. *Caenorhabditis* is a metazoan host for *Legionella*. *Cell. Microbiol.* 12:343–361. <https://doi.org/10.1111/j.1462-5822.2009.01398.x>
- Bright, N.A., M.J. Gratian, and J.P. Luzio. 2005. Endocytic delivery to lysosomes mediated by concurrent fusion and kissing events in living cells. *Curr. Biol.* 15:360–365. <https://doi.org/10.1016/j.cub.2005.01.049>
- Bright, N.A., L.J. Davis, and J.P. Luzio. 2016. Endolysosomes are the principal intracellular sites of acid hydrolase activity. *Curr. Biol.* 26:2233–2245. <https://doi.org/10.1016/j.cub.2016.06.046>
- Campbell, R.E., O. Tour, A.E. Palmer, P.A. Steinbach, G.S. Baird, D.A. Zacharias, and R.Y. Tsien. 2002. A monomeric red fluorescent protein. *Proc. Natl. Acad. Sci. USA.* 99:7877–7882. <https://doi.org/10.1073/pnas.082243699>
- Cannon, G.J., and J.A. Swanson. 1992. The macrophage capacity for phagocytosis. *J. Cell Sci.* 101:907–913. <https://doi.org/10.1242/jcs.101.4.907>
- Chantranupong, L., S.M. Scaria, R.A. Saxton, M.P. Gygi, K. Shen, G.A. Wyant, T. Wang, J.W. Harper, S.P. Gygi, and D.M. Sabatini. 2016. The CASTOR proteins are arginine sensors for the mTORC1 pathway. *Cell.* 165:153–164. <https://doi.org/10.1016/j.cell.2016.02.035>
- Cheeseman, L.P., E.F. Harry, A.D. McAinsh, I.A. Prior, and S.J. Royle. 2013. Specific removal of TACC3-ch-TOG-clathrin at metaphase deregulates kinetochore fiber tension. *J. Cell Sci.* 126:2102–2113. <https://doi.org/10.1242/jcs.124834>
- Clarke, M., J. Köhler, Q. Arana, T. Liu, J. Heuser, and G. Gerisch. 2002. Dynamics of the vacuolar H⁽⁺⁾-ATPase in the contractile vacuole complex and the endosomal pathway of *Dictyostelium* cells. *J. Cell Sci.* 115:2893–2905. <https://doi.org/10.1242/jcs.115.14.2893>
- Curchoe, C.L., and U. Manor. 2017. Actin cytoskeleton-mediated constriction of membrane organelles via endoplasmic reticulum scaffolding. *ACS Biomater. Sci. Eng.* 3:2727–2732. <https://doi.org/10.1021/acsbomaterials.6b00802>
- Damiani, M.T., and M.I. Colombo. 2003. Microfilaments and microtubules regulate recycling from phagosomes. *Exp. Cell Res.* 289:152–161. [https://doi.org/10.1016/S0014-4827\(03\)00253-2](https://doi.org/10.1016/S0014-4827(03)00253-2)
- Delevoye, C., S. Miserey-Lenkei, G. Montagnac, F. Gilles-Marsens, P. Paul-Gilloteaux, F. Giordano, F. Waharte, M.S. Marks, B. Goud, and G. Raposo. 2014. Recycling endosome tubule morphogenesis from sorting endosomes requires the kinesin motor KIF13A. *Cell Rep.* 6:445–454. <https://doi.org/10.1016/j.celrep.2014.01.002>
- Du, W., Q.P. Su, Y. Chen, Y. Zhu, D. Jiang, Y. Rong, S. Zhang, Y. Zhang, H. Ren, C. Zhang, et al. 2016. Kinesin 1 drives autolysosome tubulation. *Dev. Cell.* 37:326–336. <https://doi.org/10.1016/j.devcel.2016.04.014>
- Elkin, S.R., N.W. Oswald, D.K. Reed, M. Mettlen, J.B. MacMillan, and S.L. Schmid. 2016. Ikarugamycin: a natural product inhibitor of clathrin-mediated endocytosis. *Traffic.* 17:1139–1149. <https://doi.org/10.1111/tra.12425>
- Fairn, G.D., and S. Grinstein. 2012. How nascent phagosomes mature to become phagolysosomes. *Trends Immunol.* 33:397–405. <https://doi.org/10.1016/j.it.2012.03.003>
- Gan, Q., X. Wang, Q. Zhang, Q. Yin, Y. Jian, Y. Liu, N. Xuan, J. Li, J. Zhou, K. Liu, et al. 2019. The amino acid transporter SLC-36.1 cooperates with PtdIns3P 5-kinase to control phagocytic lysosome reformation. *J. Cell Biol.* 218:2619–2637. <https://doi.org/10.1083/jcb.201901074>
- Garg, S., M. Sharma, C. Ung, A. Tuli, D.C. Barra, D.L. Hava, N. Veerapen, G.S. Besra, N. Hacohen, and M.B. Brenner. 2011. Lysosomal trafficking, antigen presentation, and microbial killing are controlled by the Arf-like GTPase Arl8b. *Immunity.* 35:182–193. <https://doi.org/10.1016/j.immuni.2011.06.009>
- Gautreau, A., K. Oguievetskaia, and C. Ungermann. 2014. Function and regulation of the endosomal fusion and fission machineries. *Cold Spring Harb. Perspect. Biol.* 6:a016832. <https://doi.org/10.1101/cshperspect.a016832>
- Gotthardt, D., H.J. Warnatz, O. Henschel, F. Brückert, M. Schleicher, and T. Soldati. 2002. High-resolution dissection of phagosome maturation reveals distinct membrane trafficking phases. *Mol. Biol. Cell.* 13:3508–3520. <https://doi.org/10.1091/mbc.e02-04-0206>
- Gray, M., and R.J. Botelho. 2017. Phagocytosis: hungry, hungry cells. *Methods Mol. Biol.* 1519:1–16. https://doi.org/10.1007/978-1-4939-6581-6_1
- Gray, M.A., C.H. Choy, R.M. Dayam, E. Ospina-Escobar, A. Somerville, X. Xiao, S.M. Ferguson, and R.J. Botelho. 2016. Phagocytosis enhances lysosomal and bactericidal properties by activating the transcription factor TFEB. *Curr. Biol.* 26:1955–1964. <https://doi.org/10.1016/j.cub.2016.05.070>
- Harding, C.V., and H.J. Geuze. 1992. Class II MHC molecules are present in macrophage lysosomes and phagolysosomes that function in the phagocytic processing of *Listeria monocytogenes* for presentation to T cells. *J. Cell Biol.* 119:531–542. <https://doi.org/10.1083/jcb.119.3.531>
- Harrison, R.E., C. Bucci, O.V. Vieira, T.A. Schroer, and S. Grinstein. 2003. Phagosomes fuse with late endosomes and/or lysosomes by extension of membrane protrusions along microtubules: role of Rab7 and RILP. *Mol. Cell. Biol.* 23:6494–6506. <https://doi.org/10.1128/MCB.23.18.6494-6506.2003>
- Henson, P.M. 2017. Cell Removal: Efferocytosis. *Annu. Rev. Cell Dev. Biol.* 33:127–144. <https://doi.org/10.1146/annurev-cellbio-111315-125315>
- Hill, T.A., C.P. Gordon, A.B. McGeachie, B. Venn-Brown, L.R. Odell, N. Chau, A. Quan, A. Mariana, J.A. Sakoff, M. Chircop, et al. 2009. Inhibition of dynamin mediated endocytosis by the dynoles--synthesis and functional activity of a family of indoles. *J. Med. Chem.* 52:3762–3773. <https://doi.org/10.1021/jm900036m>
- Hipolito, V.E.B., J.A. Diaz, K.V. Tandoc, C. Oertlin, J. Ristau, N. Chauhan, A. Saric, S. McLaughlan, O. Larsson, I. Topisirovic, and R.J. Botelho. 2019. Enhanced translation expands the endo-lysosome size and promotes antigen presentation during phagocyte activation. *PLoS Biol.* 17:e3000535. <https://doi.org/10.1371/journal.pbio.3000535>
- Hoyer, M.J., P.J. Chitwood, C.C. Ebmeier, J.F. Striepen, R.Z. Qi, W.M. Old, and G.K. Voeltz. 2018. A novel class of ER membrane proteins regulates ER-associated endosome fission. *Cell.* 175:254–265.e14. <https://doi.org/10.1016/j.cell.2018.08.030>
- Inpanathan, S., and R.J. Botelho. 2019. The lysosome signaling platform: adapting with the times. *Front. Cell Dev. Biol.* 7:113. <https://doi.org/10.3389/fcell.2019.00113>
- Jans, R., M. Sartor, M. Jadot, and Y. Poumay. 2004. Calcium entry into keratinocytes induces exocytosis of lysosomes. *Arch. Dermatol. Res.* 296:30–41. <https://doi.org/10.1007/s00403-004-0469-0>
- Jordens, I., M. Fernandez-Borja, M. Marsman, S. Dusseljee, L. Janssen, J. Calafat, H. Janssen, R. Wubbolts, and J. Neefjes. 2001. The Rab7 effector protein RILP controls lysosomal transport by inducing the recruitment of dynein-dynactin motors. *Curr. Biol.* 11:1680–1685. [https://doi.org/10.1016/S0960-9822\(01\)00531-0](https://doi.org/10.1016/S0960-9822(01)00531-0)
- Katayama, H., A. Yamamoto, N. Mizushima, T. Yoshimori, and A. Miyawaki. 2008. GFP-like proteins stably accumulate in lysosomes. *Cell Struct. Funct.* 33:1–12. <https://doi.org/10.1247/csf.07011>
- Kinchen, J.M., and K.S. Ravichandran. 2010. Identification of two evolutionarily conserved genes regulating processing of engulfed apoptotic cells. *Nature.* 464:778–782. <https://doi.org/10.1038/nature08853>
- Kirchhausen, T., D. Owen, and S.C. Harrison. 2014. Molecular structure, function, and dynamics of clathrin-mediated membrane traffic. *Cold Spring Harb. Perspect. Biol.* 6:a016725. <https://doi.org/10.1101/cshperspect.a016725>
- Krajcovic, M., S. Krishna, L. Akkari, J.A. Joyce, and M. Overholtzer. 2013. mTOR regulates phagosome and entotic vacuole fission. *Mol. Biol. Cell.* 24:3736–3745. <https://doi.org/10.1091/mbc.e13-07-0408>
- Krishna, S., W. Palm, Y. Lee, W. Yang, U. Bandyopadhyay, H. Xu, O. Florey, C.B. Thompson, and M. Overholtzer. 2016. PIKfyve regulates vacuole maturation and nutrient recovery following engulfment. *Dev. Cell.* 38:536–547. <https://doi.org/10.1016/j.devcel.2016.08.001>
- Lancaster, C.E., C.Y. Ho, V.E.B. Hipolito, R.J. Botelho, and M.R. Terebiznik. 2019. Phagocytosis: what's on the menu? *Biochem. Cell Biol.* 97:21–29. <https://doi.org/10.1139/bcb-2018-0008>
- Le Borgne, R., and B. Hoflack. 1997. Mannose 6-phosphate receptors regulate the formation of clathrin-coated vesicles in the TGN. *J. Cell Biol.* 137:335–345. <https://doi.org/10.1083/jcb.137.2.335>
- Levin, R., S. Grinstein, and J. Canton. 2016. The life cycle of phagosomes: formation, maturation, and resolution. *Immunol. Rev.* 273:156–179. <https://doi.org/10.1111/imr.12439>
- Levin-Konigsberg, R., F. Montaña-Rendón, T. Keren-Kaplan, R. Li, B. Ego, S. Mylvaganam, J.E. DiCiccio, W.S. Trimble, M.C. Bassik, J.S. Bonifacino, et al. 2019. Phagolysosome resolution requires contacts with the endoplasmic reticulum and phosphatidylinositol-4-phosphate signalling. *Nat. Cell Biol.* 21:1234–1247. <https://doi.org/10.1038/s41556-019-0394-2>
- Li, M., B. Khambu, H. Zhang, J.-H. Kang, X. Chen, D. Chen, L. Vollmer, P.-Q. Liu, A. Vogt, and X.-M. Yin. 2013. Suppression of lysosome function induces autophagy via a feedback down-regulation of MTOR complex 1 (MTORC1) activity. *J. Biol. Chem.* 288:35769–35780. <https://doi.org/10.1074/jbc.M113.511212>
- Liebl, D., and G. Griffiths. 2009. Transient assembly of F-actin by phagosomes delays phagosome fusion with lysosomes in cargo-overloaded macrophages. *J. Cell Sci.* 122:2935–2945. <https://doi.org/10.1242/jcs.048355>
- Ludwig, T., H. Munier-Lehmann, U. Bauer, M. Hollinshead, C. Ovitt, P. Lobel, and B. Hoflack. 1994. Differential sorting of lysosomal enzymes in

- mannose 6-phosphate receptor-deficient fibroblasts. *EMBO J.* 13:3430–3437. <https://doi.org/10.1002/j.1460-2075.1994.tb06648.x>
- Ma, H., J.E. Croudace, D.A. Lammas, and R.C. May. 2006. Expulsion of live pathogenic yeast by macrophages. *Curr. Biol.* 16:2156–2160. <https://doi.org/10.1016/j.cub.2006.09.032>
- Maniak, M. 2003. Fusion and fission events in the endocytic pathway of *Dictyostelium*. *Traffic.* 4:1–5. <https://doi.org/10.1034/j.1600-0854.2003.40101.x>
- Mantegazza, A.R., J.G. Magalhaes, S. Amigorena, and M.S. Marks. 2013. Presentation of phagocytosed antigens by MHC class I and II. *Traffic.* 14: 135–152. <https://doi.org/10.1111/tra.12026>
- Mantegazza, A.R., A.L. Zajac, A. Twelvetrees, E.L.F. Holzbaur, S. Amigorena, and M.S. Marks. 2014. TLR-dependent phagosome tubulation in dendritic cells promotes phagosome cross-talk to optimize MHC-II antigen presentation. *Proc. Natl. Acad. Sci. USA.* 111:15508–15513. <https://doi.org/10.1073/pnas.1412998111>
- McCluskey, A., J.A. Daniel, G. Hadzic, N. Chau, E.L. Clayton, A. Mariana, A. Whiting, N.N. Gorgani, J. Lloyd, A. Quan, et al. 2013. Building a better dynasore: the dyngo compounds potently inhibit dynamin and endocytosis. *Traffic.* 14:1272–1289. <https://doi.org/10.1111/tra.12119>
- Mettlen, M., T. Pucadyil, R. Ramachandran, and S.L. Schmid. 2009. Dissecting dynamin's role in clathrin-mediated endocytosis. *Biochem. Soc. Trans.* 37:1022–1026. <https://doi.org/10.1042/BST0371022>
- Naufer, A., V.E.B. Hipolito, S. Ganesan, A. Prashar, V. Zaremborg, R.J. Botelho, and M.R. Terebiznik. 2018. pH of endophagosomes controls association of their membranes with Vps34 and PtdIns(3)P levels. *J. Cell Biol.* 217:329–346. <https://doi.org/10.1083/jcb.201702179>
- Parihar, A., T.D. Eubank, and A.I. Doseff. 2010. Monocytes and macrophages regulate immunity through dynamic networks of survival and cell death. *J. Innate Immun.* 2:204–215. <https://doi.org/10.1159/000296507>
- Pauwels, A.-M., M. Trost, R. Beyaert, and E. Hoffmann. 2017. Patterns, receptors, and signals: regulation of phagosome maturation. *Trends Immunol.* 38:407–422. <https://doi.org/10.1016/j.it.2017.03.006>
- Poirier, M.B., C. Fiorino, T.K. Rajasekar, and R.E. Harrison. 2020. F-actin flashes on phagosomes mechanically deform contents for efficient digestion in macrophages. *J. Cell Sci.* 133:jcs.239384. <https://doi.org/10.1242/jcs.239384>
- Prashar, A., S. Bhatia, D. Gigliozzi, T. Martin, C. Duncan, C. Guyard, and M.R. Terebiznik. 2013. Filamentous morphology of bacteria delays the timing of phagosome morphogenesis in macrophages. *J. Cell Biol.* 203:1081–1097. <https://doi.org/10.1083/jcb.201304095>
- Ramachandra, L., R. Song, and C.V. Harding. 1999. Phagosomes are fully competent antigen-processing organelles that mediate the formation of peptide: class II MHC complexes. *J. Immunol.* 162:3263–3272.
- Ripoll, L., X. Heiligenstein, I. Hurbain, L. Domingues, F. Figon, K.J. Petersen, M.K. Dennis, A. Houdusse, M.S. Marks, G. Raposo, and C. Delevoye. 2018. Myosin VI and branched actin filaments mediate membrane constriction and fission of melanosomal tubule carriers. *J. Cell Biol.* 217: 2709–2726. <https://doi.org/10.1083/jcb.201709055>
- Robinson, M.S., and J. Hirst. 2013. Rapid inactivation of proteins by knock-sideways. *Curr. Protoc. Cell Biol.* 61:20.1–7.
- Robinson, M.S., D.A. Sahlender, and S.D. Foster. 2010. Rapid inactivation of proteins by rapamycin-induced rerouting to mitochondria. *Dev. Cell.* 18: 324–331. <https://doi.org/10.1016/j.devcel.2009.12.015>
- Rong, Y., M. Liu, L. Ma, W. Du, H. Zhang, Y. Tian, Z. Cao, Y. Li, H. Ren, C. Zhang, et al. 2012. Clathrin and phosphatidylinositol-4,5-bisphosphate regulate autophagic lysosome reformation. *Nat. Cell Biol.* 14:924–934. <https://doi.org/10.1038/ncb2557>
- Rowland, A.A., P.J. Chitwood, M.J. Phillips, and G.K. Voeltz. 2014. ER contact sites define the position and timing of endosome fission. *Cell.* 159: 1027–1041. <https://doi.org/10.1016/j.cell.2014.10.023>
- Saffi, G.T., and R.J. Botelho. 2019. Lysosome fission: planning for an exit. *Trends Cell Biol.* 29:635–646. <https://doi.org/10.1016/j.tcb.2019.05.003>
- Saric, A., V.E.B. Hipolito, J.G. Kay, J. Canton, C.N. Antonescu, and R.J. Botelho. 2016. mTOR controls lysosome tubulation and antigen presentation in macrophages and dendritic cells. *Mol. Biol. Cell.* 27:321–333. <https://doi.org/10.1091/mbc.e15-05-0272>
- Saxton, R.A., L. Chantranupong, K.E. Knockenbauer, T.U. Schwartz, and D.M. Sabatini. 2016. Mechanism of arginine sensing by CASTOR1 upstream of mTORC1. *Nature.* 536:229–233. <https://doi.org/10.1038/nature19079>
- Schindelin, J., I. Arganda-Carreras, E. Frise, V. Kaynig, M. Longair, T. Pietzsch, S. Preibisch, C. Rueden, S. Saalfeld, B. Schmid, et al. 2012. Fiji: an open-source platform for biological-image analysis. *Nat. Methods.* 9: 676–682. <https://doi.org/10.1038/nmeth.2019>
- Stauffer, T.P., S. Ahn, and T. Meyer. 1998. Receptor-induced transient reduction in plasma membrane PtdIns(4,5)P₂ concentration monitored in living cells. *Curr. Biol.* 8:343–346. [https://doi.org/10.1016/S0960-9822\(98\)70135-6](https://doi.org/10.1016/S0960-9822(98)70135-6)
- Stewart, J.R., and R.A. Weisman. 1972. Exocytosis of latex beads during the encystment of *Acanthamoeba*. *J. Cell Biol.* 52:117–130. <https://doi.org/10.1083/jcb.52.1.117>
- Stoorvogel, W., V. Oorschot, and H.J. Geuze. 1996. A novel class of clathrin-coated vesicles budding from endosomes. *J. Cell Biol.* 132:21–33. <https://doi.org/10.1083/jcb.132.1.21>
- Traub, L.M., S.I. Bannykh, J.E. Rodel, M. Aridor, W.E. Balch, and S. Kornfeld. 1996. AP-2-containing clathrin coats assemble on mature lysosomes. *J. Cell Biol.* 135:1801–1814. <https://doi.org/10.1083/jcb.135.6.1801>
- van Furth, R., and Z.A. Cohn. 1968. The origin and kinetics of mononuclear phagocytes. *J. Exp. Med.* 128:415–435. <https://doi.org/10.1084/jem.128.3.415>
- von Kleist, L., W. Stahlschmidt, H. Bulut, K. Gromova, D. Puchkov, M.J. Robertson, K.A. MacGregor, N. Tomilin, A. Pechstein, N. Chau, et al. 2011. Role of the clathrin terminal domain in regulating coated pit dynamics revealed by small molecule inhibition. *Cell.* 146:471–484. <https://doi.org/10.1016/j.cell.2011.06.025>
- Werb, Z., and Z.A. Cohn. 1972. Plasma membrane synthesis in the macrophage following phagocytosis of polystyrene latex particles. *J. Biol. Chem.* 247:2439–2446. [https://doi.org/10.1016/S0021-9258\(19\)45448-3](https://doi.org/10.1016/S0021-9258(19)45448-3)
- Xu, J., K.A. Toops, F. Diaz, J.M. Carvajal-Gonzalez, D. Gravotta, F. Mazzoni, R. Schreiner, E. Rodriguez-Boulan, and A. Lakkaraju. 2012. Mechanism of polarized lysosome exocytosis in epithelial cells. *J. Cell Sci.* 125:5937–5943. <https://doi.org/10.1242/jcs.109421>
- Yu, L., C.K. McPhee, L. Zheng, G.A. Mardones, Y. Rong, J. Peng, N. Mi, Y. Zhao, Z. Liu, F. Wan, et al. 2010. Termination of autophagy and reformation of lysosomes regulated by mTOR. *Nature.* 465:942–946. <https://doi.org/10.1038/nature09076>
- Zent, C.S., and M.R. Elliott. 2017. Maxed out macs: physiologic cell clearance as a function of macrophage phagocytic capacity. *FEBS J.* 284:1021–1039. <https://doi.org/10.1111/febs.13961>
- Zoncu, R., L. Bar-Peled, A. Efeyan, S. Wang, Y. Sancak, and D.M. Sabatini. 2011. mTORC1 senses lysosomal amino acids through an inside-out mechanism that requires the vacuolar H⁽⁺⁾-ATPase. *Science.* 334:678–683. <https://doi.org/10.1126/science.1207056>

Supplemental material

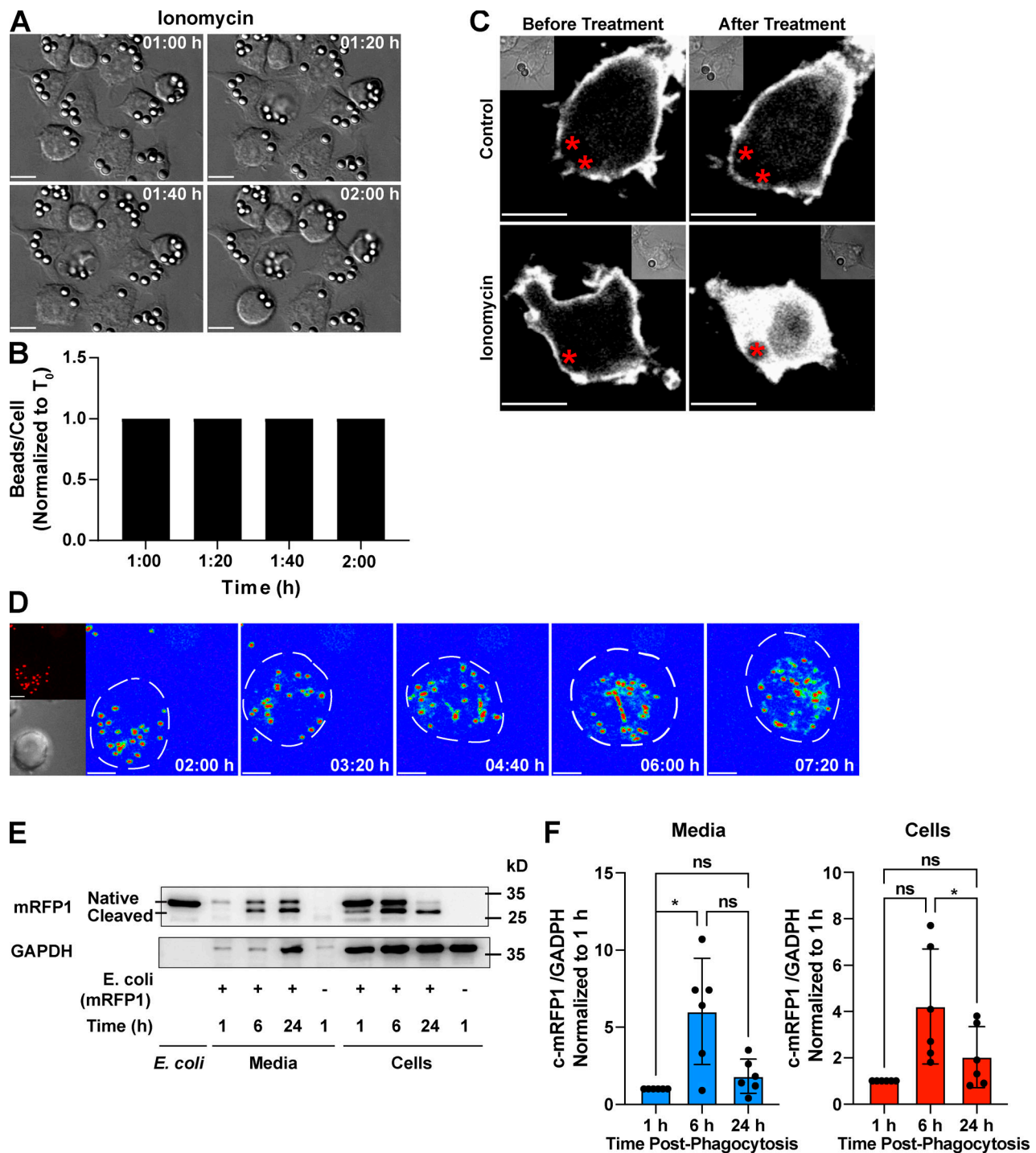


Figure S1. **Phagolysosomes do not undergo exocytosis but fragment.** (A) 1 h after phagocytosis of IgG-opsonized beads, RAW cells were treated with 10 μ M ionomycin in the presence of 1.2 mM of Ca^{2+} , and live-cell DIC images were acquired at the indicated time points. Scale bars: 10 μ m. (B) Number of latex beads per cell at the indicated treatment times, normalized to the number of beads/cell observed at the onset of the treatment (T_0). Data are mean \pm SEM of 3 independent experiments, where 10 cells were measured in each experiment. (C) RAW cells expressing PLC δ 1-PH-GFP and containing IgG-opsonized beads in phagosomes were treated with 10 μ M ionomycin or DMSO (control) in the presence of 1.2 mM of Ca^{2+} . Images were acquired before or after 10 min of treatment. Asterisks correspond to the positions of the beads, as shown in the insets. Scale bars: 10 μ m. (D) Live-cell imaging time series of IgG-aggregated fluorescent 0.1- μ m latex beads after 2-h phagocytosis by RAW cells. Beads are depicted in a rainbow scale. Red and blue correspond to the highest and lowest fluorescence intensity levels, respectively. The smaller panels show the far red and DIC channels for the first frame. The cell contour is delineated with white dashes. See corresponding Video 4. Scale bars: 5 μ m. (E) Macrophages were assessed for exocytosis of digested phagosomal contents. RAW macrophages internalized mRFP1-labeled *E. coli* for 1 h and then were incubated for the indicated time points. TCA precipitates of cell media and cell lysates were probed for mRFP1, detecting a native and a cleaved mRFP1 product that accumulated over time. GAPDH was used as a loading control and to detect cell lysis. (F) Quantification of cleaved mRFP1 levels normalized to GAPDH in media and within cells. Data are shown as mean \pm SD of six independent experiments. Conditions were compared using one-way ANOVA and Holm-Sidak's post hoc test (*, $P < 0.05$).

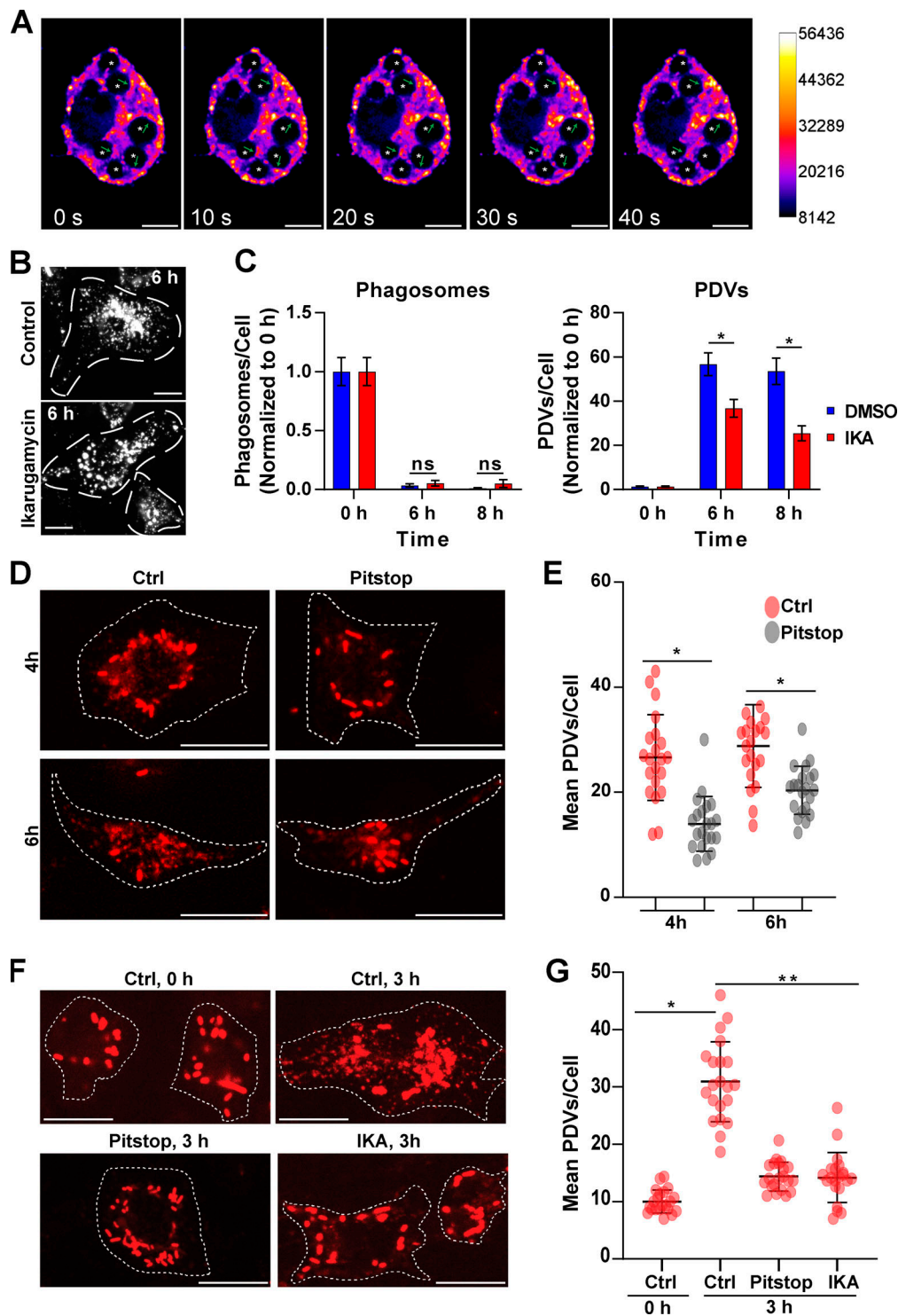


Figure S2. **Clathrin inhibition blocks phagosome resolution.** (A) Single-cell live-cell imaging time series of RAW cell expressing CLC-GFP showing internalized IgG-opsonized beads at 3 h after phagocytosis. Color scale indicates the fluorescence intensity of clathrin GFP. Time interval between frames is 10 s. Asterisk indicates internal beads, and green arrows indicate accumulation of clathrin around phagosomes. Scale bars: 5 μ m. (B) RAW cells internalized mRFP1-*E. coli* for 1 h before treatment with ikarugamycin. Live-cell imaging commenced after uptake (0 h) or >6 h after phagocytosis. (C) Intact phagosomes and PDVs per cell were quantified as puncta (particle number) for experiments displayed in B and normalized to 0 h. Data are shown as mean \pm SEM of 15 images per control/treatment across 3 independent experiments, where each image display 8–29 cells. Control and inhibitor-treated cells at each time point were compared statistically using two-way ANOVA with Sidak’s post hoc test (*, $P < 0.05$). (D) RAW macrophages internalized mRFP1-*E. coli*, were chased for 1 h, and then were treated with either vehicle or 10 μ M Pitstop 4 or 6 h after phagocytosis. (E) Primary macrophages were presented with mRFP1-*E. coli* and were treated with vehicle, Pitstop, or ikarugamycin after maturation. Cells were fixed and imaged 3 h after phagocytosis. Dashed lines show cell contours in B, D, and F. Scale bars: 10 μ m (B, D, and F). (E and G) PDVs/cell were quantified in 60 cells per condition across 3 independent experiments and compared statistically using one-way ANOVA with Dunnett’s multiple comparison test. (*, $P < 0.001$; **, $P < 0.0001$).

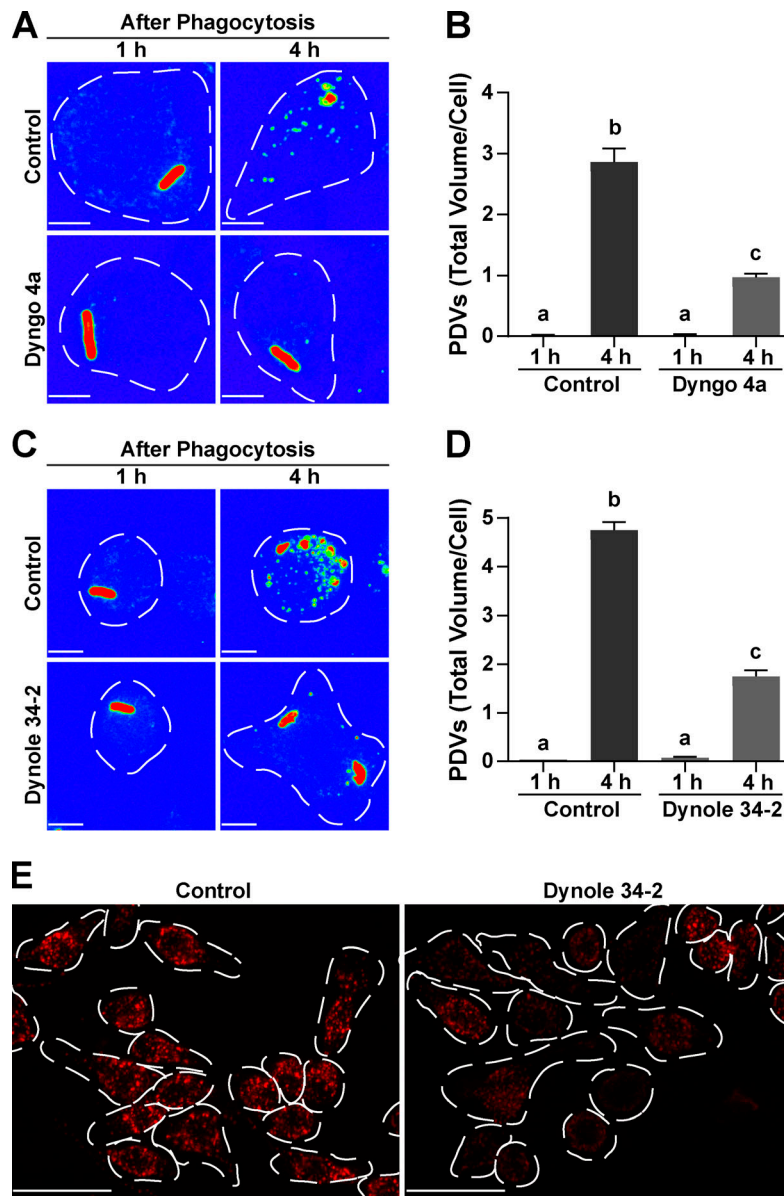


Figure S3. **Dynamin inhibition blocks phagosome fragmentation.** (A and C) 40 min after phagocytosis of mRFP1-*E. coli*, RAW cells were treated with the dynamin inhibitors dyngo-4a, dynole 34-2, or vehicle (DMSO); fixed at the indicated time points; and immunostained for *E. coli*. *E. coli* fluorescence labeling is shown in rainbow scale. Red and blue are the highest and lowest intensity levels, respectively. Dashed lines indicate the boundary of the cells. Scale bars: 5 μ m. (B and D) The total volume of PDVs per cell for the indicated treatments. Data are mean \pm SEM of sample of 25 cells from 3 independent experiments. Treatments were compared statistically using a one-way ANOVA with Tukey's post hoc test. Conditions with different letters (a-c) indicate statistically significant difference ($P < 0.05$). (E) Macrophages treated with dynole 34-2 or DMSO (vehicle) internalized Alexa Fluor 546-labeled transferrin for 10 min before fixation. White dashes indicate cell boundaries. Scale bars: 30 μ m.

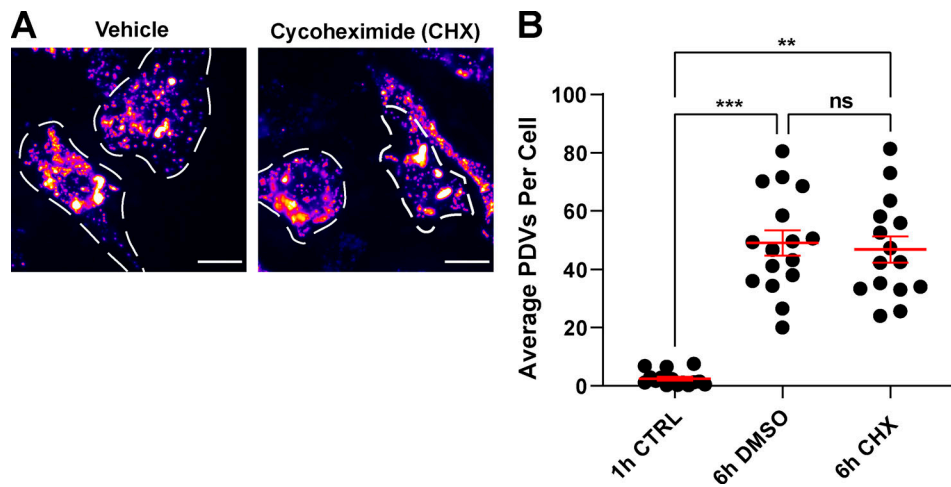


Figure S4. **The role of the biosynthetic pathway in phagosome resolution and degradative capacity of macrophages.** (A) RAW cells internalized mRFP1-*E. coli* for 20 min, and, after a 1-h chase, cells were treated with vehicle or cycloheximide (CHX) for 6 h total. Scale bars: 5 μ m. (B) Number of PDVs per cell from A shown as mean \pm SEM from groups of 15 images, each containing between 5 and 15 cells, from 3 independent experiments. Statistical analysis by one-way ANOVA with Tukey's post hoc test (**, $P < 0.01$; ***, $P < 0.001$).

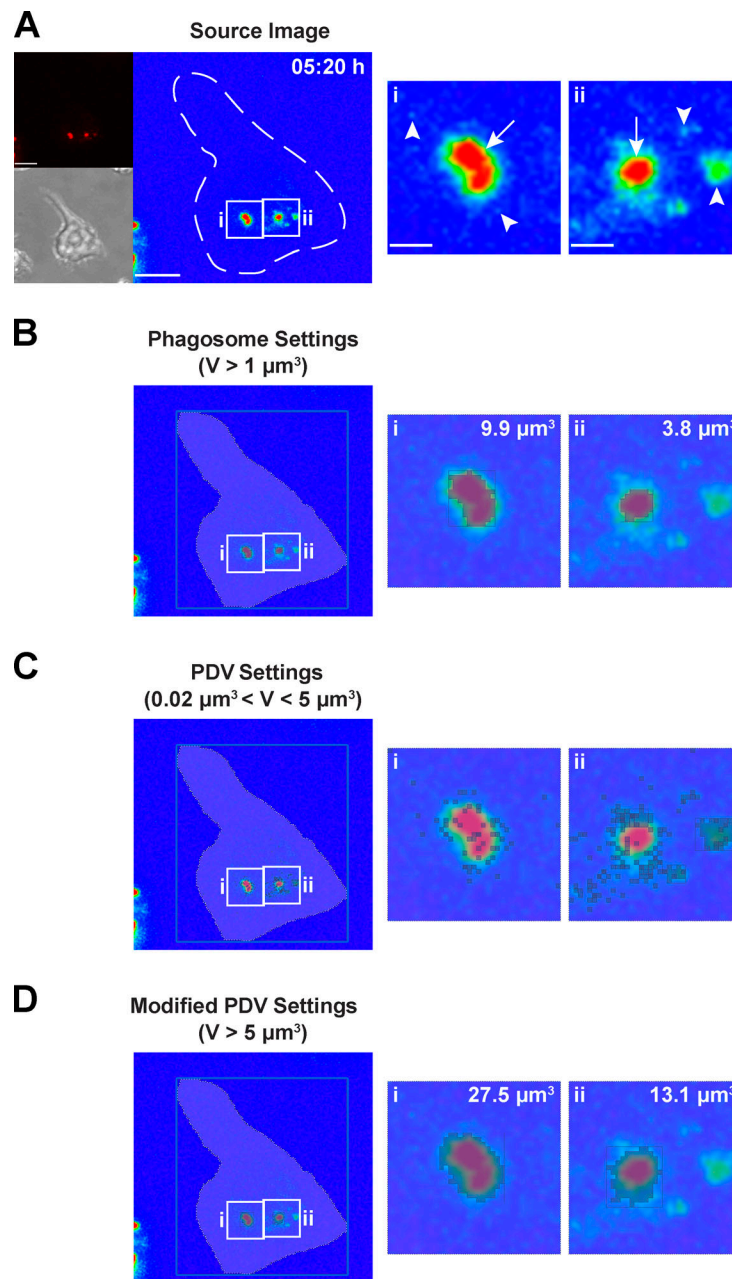


Figure S5. **Overview of the quantification method used to determine the total volume of phagosomes and PDVs in each cell.** **(A)** A still image from the same video displayed in Fig. 1 D is used to exemplify the quantification method. The main panel shows the red channel in a rainbow scale, where red is the highest intensity level and blue is the lowest intensity level. The smaller panels show the red and DIC channels. The white dashed line indicates the boundary of the cell, and the white boxes indicate the positions of the insets. Arrows within the insets point to phagosomes, while arrowheads point to PDVs. Scale bars: 10 μm (main panels), 2 μm (insets). **(B)** To quantify the total volume (V) of phagosomes in each cell, we drew a region of interest around the cell and instructed Volocity to select objects within that region, which had a high fluorescence intensity and a volume $>1 \mu\text{m}^3$ (phagosomes are under the masked areas). The volumes of the phagosomes in each region of interest were summed to determine the total volume of phagosomes in each cell. The volumes of the phagosomes displayed in the insets are indicated. **(C)** To quantify the total volume of PDVs in each cell, we instructed Volocity to select dimmer objects within the region of interest enclosing the cell, which had a volume $>0.02 \mu\text{m}^3$ but $<5 \mu\text{m}^3$ (PDVs are under the masked areas). The volumes of the PDVs in each region of interest were summed to determine the total volume of PDVs in each cell. Phagosomes were excluded from the PDV quantification because lower fluorescence intensity PDVs immediately surrounding the phagosomes were included in the phagosomal volume, which increased the apparent size of the phagosomes above the PDV threshold. **(D)** To demonstrate that the enlarged phagosomes are excluded from the PDV quantification in C, we modified the PDV settings to select the objects that had a volume $>5 \mu\text{m}^3$. The volumes of these enlarged phagosomes are indicated for comparison with phagosomes quantified in B.

Video 1. **Bead-containing phagosomes remain within macrophages over 24 h.** RAW macrophages were allowed to internalize IgG-opsonized latex beads for 2 h before cells were moved to a prewarmed (37°C) microscope stage. Images were acquired at a rate of 1 frame/h for a 24-h period. Playback rate is 4 frames/s. Still frames from [Video 1](#) are displayed in [Fig. 1 A](#). Scale bar: 10 μm .

Video 2. **Phagosomes containing mCherry-*Legionella* undergo fragmentation.** RAW macrophages were challenged with IgG-opsonized, filamentous mCherry-*Legionella* for 7 h before the cells were moved to a prewarmed (37°C) microscope stage. Images were acquired at a rate of 6 frames/h for a 13-h period. The mCherry fluorescence intensity is displayed as a rainbow scale, where red is the highest intensity level and blue is the lowest intensity level. Playback rate is 3 frames/s. Still frames from [Video 2](#) are displayed in [Fig. 1 C](#). Scale bar: 2 μm .

Video 3. **Fission of phagosomes containing ZsGreen-*E. coli*.** Macrophages were allowed to internalize ZsGreen-*E. coli*, and imaging was started immediately. Left panel shows the macrophages in DIC. Right panel shows ZsGreen fluorescent proteins from *E. coli*-containing phagosomes and phagosome-derived vesicles. Images were acquired at a rate of 2 frames/h for a 10-h period. Playback rate is 2 frames/s. [Video 3](#) is complementary to [Fig. 1 D](#). Scale bars: 10 μm .

Video 4. **Phagosomes containing fluorescent bead clumps undergo fragmentation.** Cy5-labeled 0.1- μm beads were clumped using human IgG and were presented to RAW macrophages for 2 h before the cells were moved to a prewarmed (37°C) microscope stage. Images were acquired at a rate of 3 frames/h for a 6-h period. The Cy5 fluorescence intensity is illustrated as a rainbow scale where red is the highest intensity level and blue is the lowest intensity level. Playback rate is 3 frames/s. Still frames from [Video 4](#) are displayed in [Fig. S1 D](#). Scale bar: 2 μm .

Video 5. **Budding of phagosomes containing intact mRFP1-*E. coli*.** Macrophages were allowed to internalize mRFP1-*E. coli*, and imaging was started 15 min after phagocytosis. mRFP1-positive vesicles are pseudocolored to enhance visibility of low-intensity events. Images were acquired at 1 frame every 3 s. Playback rate is 2 frames/s. Still frames from [Video 5](#) are displayed in [Fig. 3 A](#). Scale bar: 2 μm .

Video 6. **Budding of phagosomes containing degraded mRFP1-*E. coli*.** Macrophages were allowed to internalize mRFP1-*E. coli*, and imaging was started 180 min after phagocytosis. mRFP1-positive vesicles are pseudocolored to enhance visibility of low-intensity events. Images were acquired at 1 frame every 3 s. Playback rate is 2 frames/s. Still frames from [Video 6](#) are displayed in [Fig. 3 A'](#). Scale bar: 2 μm .

Video 7. **Tubulation of phagosomes containing mRFP1-*E. coli*.** Macrophages were allowed to internalize mRFP1-*E. coli*, and imaging was started 180 min after phagocytosis. mRFP1-positive vesicles are pseudocolored to enhance visibility of low-intensity events. Images were acquired at 1 frame every 3 s. Playback rate is 2 frames/s. Still frames from [Video 7](#) are displayed in [Fig. 3 B](#). Scale bar: 2 μm .

Video 8. **Splitting of phagosomes containing mRFP1-*E. coli*.** Macrophages were allowed to internalize mRFP1-*E. coli*, and imaging was started 150 min after phagocytosis. mRFP1-positive vesicles are pseudocolored to enhance visibility of low-intensity events. Images were acquired at 1 frame every 3 s. Playback rate is 2 frames/s. Still frames from [Video 8](#) are displayed in [Fig. 3 C](#). Scale bar: 2 μm .

Video 9. **Clathrin-GFP puncta associates with phagosomes and phagosome fission sites.** RAW macrophages expressing CLC-GFP engulfed mRFP1-*E. coli*. After at least 1 h of phagosome maturation, cells were imaged by spinning-disk confocal microscopy to acquire five z-planes spaced at 0.4 μm every 5 s for 5 min. Shown are collapsed z-stacks of the green and red channels. Playback rate is 3 frames/s. Still frames from [Video 9](#) are displayed in [Fig. 4 B](#). Scale bar: 5 μm .

Video 10. **Inhibition of clathrin using Pitstop prevents the fragmentation of phagolysosomes containing mCherry-*Legionella*.** RAW macrophages were allowed to internalize IgG-opsonized, filamentous mCherry-*Legionella* for 4 h before cells were moved to a prewarmed (37°C) microscope stage. After acclimatization, the cells were exposed to media containing vehicle control (DMSO) or 10 μM Pitstop 2, and imaging was started 10 min after treatment. Images were acquired at a rate of 12 frames/h for a 9.5-h period. The mCherry fluorescence intensity is illustrated in rainbow scale, where red is the highest intensity level and blue is the lowest intensity level. Playback rate is 3 frames/s. Still frames from [Video 10](#) are displayed in [Fig. 5 A](#). Scale bar: 2 μm .